The Astronomical Journal, 149:52 (22pp), 2015 February doi:10.1088/0004-6256/149/2/52

DEEP WASHINGTON PHOTOMETRY OF INCONSPICUOUS STAR CLUSTER CANDIDATES IN THE LARGE MAGELLANIC CLOUD

Samyaday Choudhury[1,2], Annapurni Subramaniam[1], and Andrés E. Piatti[3,4]
[1] Indian Institute of Astrophysics, 2B Koramangala, Bangalore 560034, India; samyaday@iiap.res.in
[2] Indian Institute of Science, Bangalore 560012, India
[3] Observatorio Astronómico, Universidad Nacional de Córdoba, Laprida 854, X5000BGR, Córdoba, Argentina
[4] Consejo Nacional de Investigaciones Científicas y Técnicas, Avenida Rivadavia 1917, C1033AAJ, Buenos Aires, Argentina
Received 2014 August 25; accepted 2014 October 24; published 2015 January 15

ABSTRACT

We present deep Washington photometry of 45 poorly populated star cluster candidates in the Large Magellanic Cloud (LMC). We have performed a systematic study to estimate the parameters of the cluster candidates by matching theoretical isochrones to the cleaned and dereddened cluster color–magnitude diagrams. We were able to estimate the basic parameters for 33 clusters, out of which 23 are identified as single clusters and 10 are found to be members of double clusters. The other 12 cluster candidates have been classified as possible clusters/asterisms. About 50% of the true clusters are in the 100–300 Myr age range, whereas some are older or younger. We have discussed the distribution of age, location, and reddening with respect to field, as well as the size of true clusters. The sizes and masses of the studied sample are found to be similar to that of open clusters in the Milky Way. Our study adds to the lower end of cluster mass distribution in the LMC, suggesting that the LMC, apart from hosting rich clusters, also has formed small, less massive open clusters in the 100–300 Myr age range.

Key words: galaxies: individual (LMC) – galaxies: star clusters: general – Magellanic Clouds – techniques: photometric

1. INTRODUCTION

Star clusters in the Large Magellanic Cloud (LMC) have been the target of detailed study to understand several processes such as star formation and chemical evolution of the galaxy (Olszewski et al. 1991; Pietrzyński & Udalski 2000; Grocholski et al. 2006). The LMC hosts a large number of star clusters, and the most recent and extensive catalog of known clusters in the Magellanic Clouds is given by Bica et al. (2008, hereafter B08). However, the cluster sample, as mentioned by the authors, is still incomplete. Most of the previous studies of LMC star clusters have targeted rich clusters that stand out from the field due to their high stellar density. Two of the profound studies of LMC star clusters using color–magnitude diagrams (CMDs) are by Pietrzyński & Udalski (2000, hereafter PU00) and Glatt et al. (2010, hereafter G10). PU00 estimated the ages of about 600 clusters using the Optical Gravitational Lensing Experiment (OGLE) II data, whereas G10 identified 1193 star clusters and estimated their ages using the Magellanic Cloud Photometric Survey (MCPS, Zaritsky et al. 2004) data. Both PU00 and G10 had carried out their work primarily for young clusters aged less than 1 Gyr, aiming to understand the cluster formation history. Another method that is generally employed to estimate the masses and ages of clusters for a sufficiently large number of samples is the use of integrated photometry; see, e.g., Hunter et al. (2003) and Popescu et al. (2012). Popescu et al. (2012, hereafter P12) estimated the age and mass for 920 LMC clusters based on previously published broadband photometry and the stellar cluster analysis package, MASSCLEANage.

Apart from rich clusters, the LMC also hosts a large number of clusters that have relatively fewer number of stars, similar to the open clusters of our Galaxy. Despite the aforementioned extensive studies, these category of clusters are, in general, either unstudied or poorly studied, due to lack of deep photometric data. As these sparse clusters are also part of the cluster system of the LMC, it is necessary to study them in order to understand the cluster formation and survival processes. The recent works of Piatti (2012, 2014) and Palma et al. (2013) were directed toward increasing the sample of poorly studied/unstudied clusters in the LMC. They used the cluster CMDs to estimate ages for such cluster candidates in the LMC using deep Washington photometry.

In this study, we attempt to increase our understanding of inconspicuous stars clusters in the LMC using deep Washington photometric data. The current study thus aims at increasing the number of studied clusters and disentangling the possible asterisms from genuine clusters. We have carried out a homogeneous analysis of 45 LMC clusters using deep photometric data in the Washington system. As is well known, the Washington photometric system has been widely applied to studies of intermediate-age and old clusters in the Galaxy and in the Magellanic Clouds (e.g., Geisler et al. 1997; Geisler & Sarajedini 1999; Piatti et al. 2003; Piatti 2012). Particularly, the depth reached by the present photometric data helps us to trace the poorly populated clusters as well as the fainter end of the main sequence of sparse clusters.

The paper is organized as follows. Section 2 deals with the acquisition and reduction of the aforementioned Washington photometric data. Section 3 describes the methods adopted for estimating the cluster parameters (radius, reddening, and age). In Section 4, we present the results derived from our analysis and discuss the same in Section 5. We summarize our findings in Section 6.

2. DATA

This paper is a continuation of our series of studies about LMC cluster candidates (Piatti et al. 2009, 2011; Palma et al. 2013; Piatti 2011, 2012, 2014) using the CT_1 Washington photometric system (Canterna 1976; Geisler 1996). In this study, we focus on the 45 LMC star cluster candidates for

which Washington C and Kron–Cousins R data were retrieved from the National Optical Astronomy Observatory (NOAO) Science Data Management Archives.[5] The cluster sample was selected from the cataloged clusters identified by Piatti (2011) in the 21 LMC fields observed at the Cerro-Tololo Inter-American Observatory 4 m Blanco telescope with the Mosaic II camera attached (36×36 arcmin^2 field onto a 8K × 8K CCD detector array), through program 2008B-0912 (PI: D. Geisler). The volume of images includes calibration frames (zeros, sky-flats, etc.) and standard and program fields observed through the Washington C and Kron–Cousins R, I filters. Note that the R filter has a significantly higher throughput as compared to the standard Washington T_1 filter so that R magnitudes can be accurately transformed to yield T_1 magnitudes (Geisler 1996).

The data were reduced following the procedures documented by the NOAO Deep Wide-Field Survey team (Jannuzi et al. 2003) by using the MSCRED package in IRAF.[6] The different tasks performed went through overscan, trimming and cross-talk corrections, and bias subtraction; obtained an updated world coordinate system database; and flattened all data images, etc., once the calibration frames (zeros, sky- and dome-flats, etc.) were properly combined. Nearly 90 independent measures of standard stars were derived per filter for each of the 3 nights (2008 December 18–20) during which the observations were carried out in order to obtain the coefficients of the transformation equations:

$$c = a_1 + T_1 + (C - T_1) + a_2 \times X_C + a_3 \times (C - T_1), \quad (1)$$

$$r = b_1 + T_1 + b_2 \times X_R + b_3 \times (C - T_1), \quad (2)$$

$$i = c_1 + T_1 - (T_1 - T_2) + c_2 \times X_I + c_3 \times (T_1 - T_2), \quad (3)$$

where a_i, b_i, and c_i ($i = 1$, 2, and 3) are the fitted coefficients, and X represents the effective airmass. Capital and lowercase letters represent standard and instrumental magnitudes, respectively. These equations were solved with the FITPARAMS task in IRAF, and mean color terms (a_3, b_3, and c_3) resulted as –0.090 ± 0.003 in C, –0.020 ± 0.001 in T_1, and 0.060 ± 0.004 in T_2, whereas typical airmass coefficients (a_2, b_2, c_2) resulted in 0.31, 0.09, and 0.06 for C, T_1, and T_2, respectively. The nightly rms errors from the transformation to the standard system were 0.021, 0.023, and 0.017 mag for C, T_1, and T_2, respectively, indicating these nights were of excellent photometric quality.

The star-finding and point-spread function (PSF) fitting routines in the DAOPHOT/ALLSTAR suite of programs (Stetson et al. 1990) were used with the aim of performing the stellar photometry. For each frame, we selected ∼960 stars to fit a quadratically varying PSF, once the neighbors were eliminated using a preliminary PSF derived from the brightest, least contaminated ∼240 stars. Both groups of PSF stars were interactively selected. We then used the ALLSTAR program to apply the resulting PSF to the identified stellar objects and to create a subtracted image, which was used to find and to measure magnitudes of additional fainter stars. This procedure was repeated three times for each frame. Finally, we standardized the resulting instrumental magnitudes and combined all the independent measurements using the stand-alone DAOMATCH and DAOMASTER programs, kindly provided by Peter Stetson. The final information gathered for each cluster consists of a running number per star, the X and Y coordinates, the measured T_1 magnitudes and $C - T_1$ and $T_1 - T_2$ colors, and the observational errors $\sigma(T_1)$, $\sigma(C - T_1)$ and $\sigma(T_1 - T_2)$.

[5] http://www.noao.edu/sdm/archives.php

[6] IRAF is distributed by the National Optical Astronomy Observatories, which is operated by the Association of Universities for Research in Astronomy under contract with the National Science Foundation.

3. ESTIMATION OF CLUSTER PARAMETERS

For each of the selected cluster candidate fields, we made use of the measured stars within a radius of approximately 130″ around the central coordinates provided by B08. The cluster candidates analyzed here are relatively faint objects and are mostly unstudied. Furthermore, most of them are in turn relatively small angular-sized objects projected toward densely populated star fields. Our first step in the analysis was to estimate the radius of each cluster from their radial density profiles (RDPs). Then, the second step was to remove the field stars within the cluster radius that contaminate the cluster CMD. Finally, we dealt with estimating the age and reddening of the genuine clusters by visually fitting isochrones to the cleaned cluster CMDs. The set of isochrones used in this study come from Marigo et al. (2008), with a metallicity of $Z = 0.008$, as judged from the observed LMC metallicity range for the last 3 Gyr (Piatti & Geisler 2013).

3.1. Estimation of Cluster Center and Cluster Radius

We assume the presence of a star cluster when a stellar density enhancement is identified in the spatial distribution of field stars. For this purpose, we first created finding charts for all clusters, using measured stars with sizes proportional to their T_1 magnitudes. The cluster centers were estimated through an iterative method, starting from an eye-estimated center, (X_e, Y_e), for stars brighter than $T_1 = 22.0$ mag. We computed the average of the coordinates (X, Y) for all the stars distributed within 200 pixels around (X_e, Y_e) to estimate the central coordinate of the cluster, (X_c, Y_c). Iterations were carried out until the difference in the estimated center of two consecutive iterations was less than 10 pixels (2.7 arcsec). The number of stars per unit area in rings of 10 pixel width around the cluster center were used to build the RDPs. The RDPs were visually fitted with the King (1962) profile:

$$\rho(r) = \frac{\rho_0}{1 + (r/r_c)^2} + \rho_b, \quad (4)$$

where ρ_0 is the central density, ρ_b is the background density, and r_c is the core radius. We fix the value of ρ_0 to visually fit the peak and the value of ρ_b to visually fit the background field density of the RDP at a large radial distance. The r_c value is then adopted so as to obtain the best visual fit of the King profile to the RDP. We adopted cluster radii (r) as the distance from the cluster center at which the cluster density becomes equal to the background field density, which is taken as three times r_c. This is found to hold for most of the clusters. The clusters studied here are sparse, and hence we have used this radius to include most of the cluster members. The error in the estimation of the cluster radius is expected to be about ±10″, which is about three times the bin size used in estimating the RDP.

In clusters where there is incompleteness of bright stars in the central cluster region due to saturation, we were unable to obtain their centers from the method described above. For these clusters we adopted either the central coordinates given by B08 or the eye-estimated centers from the densest visible cluster

regions. Likewise, when we were unable to reliably determine a cluster radius by visually fitting a King profile to the RDP or were unable to estimate an RDP, we chose the radius which brings out the cluster features clearly. For some of the clusters it was difficult to define a circular area; instead we used a rectangular region where the cluster might be most probably located. It is to be noted that the convention followed while mentioning the rectangular dimension is thus: the size along the X coordinate times the size along the Y coordinate, in arcseconds.

3.2. Cleaning the Cluster CMD

In order to analyze the cluster CMDs using stars located within the adopted cluster radii, one has to remove the contamination due to the field stars by performing a statistical field star subtraction. For field star subtraction, we selected field stars within an annular region of area equal to that of the cluster, with the inner radius of the annulus around twice or more than the cluster radius. The field stars in the cluster area are then removed by taking each star in the field CMD and finding the nearest one in the cluster CMD, considering a grid of magnitude–color bins with different sizes, starting with $[\Delta T_1, \Delta(C - T_1)] = [0.01, 0.005]$ up to a maximum of [0.4, 0.2], where the units are magnitude. In order to minimize effects due to field star density fluctuations, we repeated the decontamination procedure using different annular regions for each cluster and then compared the different resultant cleaned cluster CMDs. The cleaned cluster CMDs thus primarily show the cluster features with minimum inescapable field characteristics.

In cases where we could not consider an annular field region, the field stars were removed by selecting field regions (not necessarily circular) of equal cluster area in different parts of the observed field, located away from the cluster, and performing the cleaning procedure described above. The cluster features that stay irrespective of the field used are considered as genuine cluster features and are used for estimating parameters.

3.3. Estimating Ages and Reddenings for the Cluster Sample

We determine the ages of the clusters by a visual fit of theoretical isochrones from Marigo et al. (2008) with LMC metallicity ($Z = 0.008$) to the cleaned cluster CMDs. For visually fitting theoretical isochrones to the observed CMDs, the $(C - T_1)$ colors and T_1 magnitudes need to be corrected for reddening and distance modulus, respectively. Subramaniam & Subramanian (2010) have created a reddening map for the LMC field using OGLE III data (Udalski et al. 2008). They provide $E(V - I)$ color excesses for small regions within the galaxy. For a given cluster, we find the closest region in the reddening map and assume $E(V - I)$ of the field as the cluster reddening. The average of the distance between the clusters and their closest adopted field regions in the reddening map is approximately 6 arcmin. Finally, the theoretical isochrones were shifted to the observation plane, according to Equations (5) and (6):

$$\left(C - T_1\right)_{\rm observed} = \left(C - T_1\right)_o + E\left(C - T_1\right), \qquad (5)$$

where $E(C - T_1) = 1.97\ E(B - V)$ (Geisler & Sarajedini 1999) and $E(B - V) = E(V - I)/1.25$ (Bessell & Brett 1988). The expected error in reddening is less than ± 0.05 mag, which includes the photometric error and the error in the estimation of field reddening.

$$T_{1_{\rm observed}} = M_{T_1} + 2.62E(B - V) + (m - M)_o, \qquad (6)$$

as given by Geisler & Sarajedini (1999).

We assume a true distance modulus of $(m - M)_o = 18.50$ for all of the cluster samples, recently obtained by Saha et al. (2010). The cleaned cluster CMDs were matched with different isochrones after incorporating the corrections due to reddening and distance modulus. The age of the isochrone that visually provides the best match to the observed cluster CMD was adopted as the cluster age. However, whenever a cluster exhibits a dispersion in its CMD features, particularly near the turn-off, we overplotted additional isochrones in order to take into account the observed spread. Piatti (2014) discusses the error in the estimation of age. In general, the observed dispersion seen in the cluster CMDs can be encompassed with a spread of $\Delta\log(t) \sim 0.10$. We discuss cases with a large spread in age or a large error in the age estimation separately.

4. RESULTS

We classified the studied clusters into two groups, namely, true clusters and possible clusters/asterisms. True clusters are those which have prominent cluster features (upper MS and/or MSTOs) and where one could satisfactorily estimate the cluster parameters, such as radius, age, and reddening. There are 33 such clusters, out of which 23 fields contain single clusters (Table 1) and 5 fields contain a pair of clusters (Table 2). There are 12 cases where the cluster features are either poor (only a few stars in their upper MS and MSTO) or suspicious/missing. Due to the difficulty in confirming the presence of an actual cluster in those fields and getting a satisfactory estimation of their cluster parameters, they are categorized as possible clusters/asterisms (Table 3). We have presented the finding chart, cluster CMD (before and after field star correction), and the estimated RDP (wherever possible) for all clusters in the appendix. The true single and double clusters are presented in Appendices A and B, respectively, whereas the possible cluster/asterisms are presented in Appendix C. In Tables 1, 2, and 3, we have presented the coordinates, R.A. and decl., the center of the cluster (to correlate with the finding chart), estimated cluster radius in arcseconds, reddening $E(C - T_1)$, age, earlier age estimate, and cross IDs. In Table 2, the five double clusters are listed with members of each pair grouped together.

As an example, the derived parameters and the corresponding diagram for a true single cluster, HS 411, is presented in Figure 1. In the multipanel plot, the top left panel shows the schematic chart, with the red dashed circle denoting the estimated extent of the cluster. The RDP of HS 411 is shown with a King profile in the top right panel. The bottom left panel shows the CMD of stars within the estimated radius and field stars located in the adopted field region. The inner radius of the field region chosen is also indicated in the figure. The bottom right panel shows isochrones visually fitted to the cleaned CMD of the HS 411 cluster. Similar multipanel plots have been created for all of the analyzed clusters, unless stated otherwise (see Appendices A and B).

The true clusters, listed in Tables 1 and 2, stand out either in terms of number density, features in the CMD, or both. There are clusters for which either the RDP did not show a strong peak (BSDL 631, H88-265, H88-269, and HS 247) or where

Table 1
Estimated Parameters for Single Clusters

Cluster Name	α (h m s)	δ (° ′ ″)	(X_c,Y_c) (pixels)	r (″)	$E(C-T_1)$ (mag)	log(t)	Lit.[a]	Cross ID
BRHT 45a	04 56 54	−68 00 08	(1833, 3604)	27	0.15	8.10	8.00 (1)	HS 72,
…	…	…	…	…	…	…	…	KMHK 326
BSDL 77	04 50 29	−67 19 33	(5421, 5679)	24	0.00	8.90	…	…
BSDL 268	04 55 52	−69 42 21	(5040, 3290)[a]	(64.″8 × 54″)	0.20	7.95	7.50 (1)	…
BSDL 631	05 06 34	−68 25 38	(509, 3280)	15	0.00	8.35	7.50 (1)	OGLE 109
H88-33	04 55 41	−67 47 00	(4791, 2141)	18	0.13	8.20–8.50	8.13 (3)	KMHK 286
H88-131	05 06 41	−67 50 32	(2841, 1234)	24	0.06	9.00	…	KMHK 544
H88-265	05 18 05	−69 10 18	(1521, 3570)[a]	20[b]	0.10	8.30	7.90 (2)	OGLE 323
H88-269	05 18 41	−69 04 46	(2760, 4314)	20[b]	0.10	8.90	8.80 (2)	OGLE 337
H88-320	05 41 58	−69 02 51	(5595, 2411)	27	0.33	8.20	8.00 (1)	KMHK 1248
H88-331	05 44 11	−69 20 00	(1737, 5028)	24	0.23	8.70	…	KMHK 1313
HS 116	05 06 12	−68 03 47	(5389, 2885)	18	0.08	8.55	…	KMHK 536
HS 131	05 09 12	−68 26 39	(192, 6565)	(27″ × 27″)	0.16	9.10	…	…
HS 247	05 21 45	−68 55 02	(4874, 8051)	20[b]	0.25	8.55	8.04 (3)	…
HS 390	05 41 30	−69 11 06	(3764, 1829)	20	0.45	8.25	7.92 (3)	KMHK 1239
HS 411	05 45 50	−69 22 49	(1065, 6963)	15	0.34	8.45	…	KMHK 1345
HS 412	05 45 56	−69 16 19	(2546, 7088)[a]	25[b]	0.34	8.10	8.10 (1)	KMHK1347
KMHK 95	04 47 26	−67 39 35	(809, 1705)	21	0.08	8.55	…	…
KMHK 907	05 26 12	−70 58 53	(486, 3558)	21	0.18	8.40	…	…
KMHK 975	05 29 59	−67 52 44	(7467, 582)	21	0.10	8.30	7.40 (1)	…
LW 54	04 46 04	−66 54 41	(470, 7304)	18	0.00	8.60	8.60 (1)	KMHK 72
NGC 1793	04 59 38	−69 33 27	(7068, 7815)	25[b]	0.21	8.05	8.00 (1)	SL 163,
…	…	…	…	…	…	…	…	ESO 56SC 43,
…	…	…	…	…	…	…	…	KMHK 405
SL 397	05 20 12	−68 54 15	(5076, 6175)[a]	25[b]	0.16	8.20	7.80 (1)	…
SL 579	05 34 13	−67 51 23	(7723, 5989)	18	0.13	8.15	7.80 (1)	KMHK 1085

References. Lit.[a]: (1) Glatt et al. (2010), (2) Pietrzyński & Udalski (2000), (3) Popescu et al. (2012).
[a] Implies cases where we adopted either the central coordinates given by B08 or the eye-estimated centers from the densest visible cluster regions as the cluster center.
[b] Cases where either we could not overplot the King profile to the RDP or the RDP could not be estimated. For these cases, the estimated radius is the one at which the cluster profile becomes prominent. In cases where one could not define a circular area, the possible rectangular area of the cluster is mentioned (dimension along the X coordinate times that along the Y coordinate).

we could not obtain an RDP (BSDL 268, NGC 1793, and SL 397), suggesting a poor density enhancement in the cluster region. This is likely to be due to saturation effects caused by the presence of bright stars near the cluster center, resulting in missing stars and incompleteness in the central region for these clusters. As our data could not confirm the density enhancement, we tried to identify the density enhancement using other optical data. The OGLE III is one of the complete and relatively deep surveys of the inner region of the LMC (4°–5°) with good spatial resolution. We extracted OGLE III fields corresponding to each of these clusters and created similar finding charts using V magnitude. Although the OGLE III data are helpful for young clusters with bright stars, the OGLE III data are not much help for relatively older clusters. We have discussed these cases in Appendix A.

The clusters in Table 3 (possible clusters/asterisms) fall into this group, mainly due to the inability of the present study to identify/detect any of the cluster characteristics for the stars in the cluster region. This group has two types of clusters: one type could be clusters, but we could not estimate their parameters reliably, whereas the others could not even be detected/recognized reliably as clusters. We define possible cluster candidates as those with the following properties: (1) they have marginal spatial density enhancement with respect to the field; (2) cluster features in the CMD are very poorly defined, with only a few stars in their upper MS and MSTO; and (3) there is an identifiable difference in the evolutionary features of the CMD for the cluster and field regions. The first two properties make it difficult to clearly estimate the cluster parameters, such as radius, age, and reddening, whereas the third property suggests that there may be a cluster present in the location. Asterisms are those objects with marginal or no spatial apparent density enhancement with respect to the field; the cluster features in the CMD were either suspicious or completely missing, and the CMD of the cluster and the field region appear almost similar. As there is a very thin dividing line between the two types, we have put them as one group. In our study we report 12 cases that belong to this category. Detailed discussion of individual objects and their corresponding plots (similar to that of Figure 1) is presented in Appendix C. We provide a limit on the possible spatial extent and age of these objects, if these objects are true clusters at all. Given the very sparse nature of the objects under this category, the age uncertainty could be larger ($\Delta\log(t) \sim 0.20$). To avoid clutter in the CMD we have only shown isochrones of age ± 0.10 with respect to the best visually fitted isochrone. We also took the help of the OGLE III field for verification, but these clusters are too poor to confirm them as clusters using this data. As our data are much deeper when compared to OGLE III and other survey data, the present data should have detected the presence of such poor and faint clusters. Eight out of 12 have been previously studied by either PU00, G10, or P12. We need deeper data, such as LSST, to identify the true nature of these

Table 2
Double Clusters

Cluster Name	α (h m s)	δ (° ′ ″)	(X_c,Y_c) (pixels)	r (″)	$E(C-T_1)$ (mag)	log(t)	Lit.[a]	Cross ID
BSDL 341	04 58 15	−68 02 57	(1219, 5349)	24	0.17	8.45	7.64 (3)	⋯
H88-52	04 58 10	−68 03 37	(1031, 5229)	27	0.08	9.05	8.73 (3)	KMHK 365
HS 154	05 10 56	−67 37 36	(5716, 6660)	24	0.13	8.65	8.70 (2)	H88-189,
⋯	⋯	⋯	⋯	⋯	⋯	⋯	⋯	KMHK 625,
⋯	⋯	⋯	⋯	⋯	⋯	⋯	⋯	OGLE 194
HS 156	05 11 11	−67 37 37	(5727, 6961)	21	0.13	9.05	⋯	H88-190,
⋯	⋯	⋯	⋯	⋯	⋯	⋯	⋯	KMHK 632,
⋯	⋯	⋯	⋯	⋯	⋯	⋯	⋯	OGLE 199
KMHK 979	05 29 39	−70 59 02	(387, 7390)[a]	20[b]	0.17	7.90	7.30 (1)	GKK-O101
HS 329	05 29 46	−71 00 02	(150, 7475)[a]	(37.″8× 40.″5)	0.00	8.90–9.00		KMHK 984
SL 230	05 06 34	−68 21 47	(1380, 3281)[a]	25[b]	0.16	7.90	7.40 (1)	BRHT 29b,
⋯	⋯	⋯	⋯	⋯	⋯	⋯	⋯	OGLE 107
SL 229	05 06 25	−68 22 30	(1230, 3088)[a]	21	0.12	8.50	8.35 (2)	BRHT 29a,
⋯	⋯	⋯	⋯	⋯	⋯	⋯	⋯	OGLE 105
SL 551	05 31 51	−67 59 28	(5956, 2989)	20[b]	0.18	8.15	7.90 (1)	BRHT 38a,
⋯	⋯	⋯	⋯	⋯	⋯	⋯	⋯	KMHK 1027,
⋯	⋯	⋯	⋯	⋯	⋯	⋯	⋯	GKK-O202
BRHT 38b	05 31 58	−67 58 18	(6200, 3140)[a]	(27″ × 32.″4)	0.16	8.25	8.00 (3)	KMHK 1032

References. Lit.[a]: (1) Glatt et al. (2010), (2) Pietrzyński & Udalski (2000), and (3) Popescu et al. (2012).
[a] Implies cases where we adopted either the central coordinates given by B08 or the eye-estimated centers from the densest visible cluster regions as the cluster center.
[b] Cases where either we could not overplot the King profile to the RDP or the RDP could not be estimated. For these cases, the estimated radius is the one at which the cluster profile becomes prominent. For cases where one could not define a circular area, the possible rectangular area of the cluster is mentioned (the dimension along the X coordinate times that along the Y coordinate).

Table 3
Possible Clusters and Asterisms

Cluster Name	α (h m s)	δ (° ′ ″)	(X_c,Y_c) (pixels)	r (″)	$E(C-T_1)$ (mag)	log(t)	Lit.[a]	Cross ID
BSDL 677	05 07 54	−67 55 44	(7177, 5070)[a]	21	0.08	8.25	⋯	⋯
H88-235	05 15 47	−69 11 31	(1243, 780)	15	0.12	8.75	8.55 (3)	OGLE 277
H88-244	05 16 17	−69 09 15	(1749, 1410)[a]	25[b]	0.25	8.30	8.10 (2)	OGLE 285
H88-279	05 20 02	−69 15 40	(265, 5890)[a]	20[b]	0.16	8.10	8.00 (2)	OGLE 361
H88-288	05 21 15	−69 01 43	(3403,7486)	18	0.25	8.40	8.04 (3)	⋯
H88-289	05 21 20	−69 00 30	(3674, 7521)[a]	20[b]	0.25	8.45	7.80 (3)	⋯
H88-307	05 40 26	−69 14 55	(2905, 559)[a]	(54″ × 54″)	0.30	8.25	⋯	⋯
H88-316	05 41 39	−69 13 46	(3159, 1950)[a]	(54″ × 54″)	0.30	8.25	8.00 (1)	⋯
KMHK 378	04 58 22	−69 48 11	(3608, 6451)	15	0.14	8.45	7.40 (1)	⋯
KMHK 505	05 04 33	−67 58 32	(6609, 791)	18	0.11	8.75	⋯	⋯
OGLE 298	05 16 53	−69 09 00	(1800, 2135)[a]	15	0.25	8.30	7.30 (2)	⋯
SL 269	05 09 35	−67 48 38	(3291, 4878)	25[b]	0.11	8.25	⋯	KMHK 598,
⋯	⋯	⋯	⋯	⋯	⋯	⋯	⋯	GKK-O216

References. Lit.[a]: (1) Glatt et al. (2010), (2) Pietrzyński & Udalski (2000), and (3) Popescu et al. (2012).
[a] Implies cases where we adopted either the central coordinates given by B08 or the eye-estimated centers from the densest visible cluster regions as the cluster center.
[b] Cases where either we could not overplot the King profile to the RDP or the RDP could not be estimated. For these cases, the estimated radius is the one at which the cluster profile becomes prominent. For cases where one could not define a circular area, the possible rectangular area of the cluster is mentioned (the dimension along the X coordinate times that along the Y coordinate).

clusters and also to reliably estimate the parameters of the possible clusters.

The age distribution of the 33 true clusters is shown as a histogram in Figure 2. The age is considered on a logarithmic scale, and the bin size is chosen to be equal to the typical age error in this study (i.e., $\Delta\log(t) = \pm 0.10$) so as to avoid any bias in the distribution due to error in age. For H88-33 and HS 329, where we could only find out a range in age, their mean age is considered in the histogram. It is clearly seen that approximately 50% of the clusters are in the age range log (t) = 8.0–8.5 (i.e., ∼100–300 Myr). The rest of them are either younger or older. BSDL 268, KMHK 979, and SL 230 lie at the youngest end (<100 Myr) of the age distribution. These clusters could be younger than their estimated ages, as some upper MS or MSTO stars are missing from the center of the cluster region due to the saturation effect. The clusters H88-52,

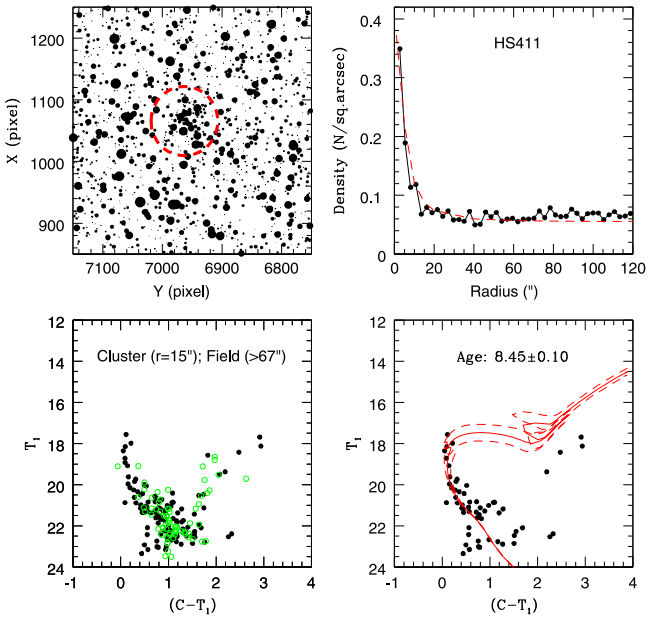

Figure 1. HS 411: (i) Top left—spatial distribution of the stars in the cluster field (north is up, and east is left), along with the estimated cluster size (red dashed circle). (ii) Top right—The King profile overplotted (red dashed line) to the RDP (black solid line). (iii) Bottom left—uncleaned cluster CMD (black filled circles) within the cluster radius, with the field CMD overplotted (green open circles). The cluster radius and the inner radius of the field are indicated. (iv) Bottom right—isochrones overplotted (red solid and dashed lines) to the cluster CMD after removal of field stars.

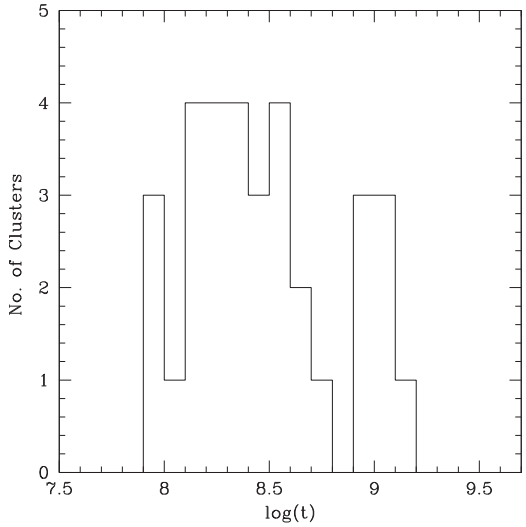

Figure 2. Age distribution of 33 true clusters.

HS 156, H88-131, and HS 131 are aged around 1 Gyr and lie at the oldest age end of the histogram.

Out of the 33 true clusters, 23 have previous age estimates. We have compared our age estimation with these previous studies of LMC clusters by PU00 and G10, who used CMDs to estimate ages using the OGLE II and the MCPS data, respectively. The limiting magnitude of their data does not allow them to detect older clusters and constrains them to only younger clusters. We also compared our results with P12, who used integrated photometry to estimate the ages of the LMC clusters mentioned in Hunter et al. (2003). With our deep photometric data we were able to go faint enough to detect older MSTOs, as well as to identify clusters with poor cluster

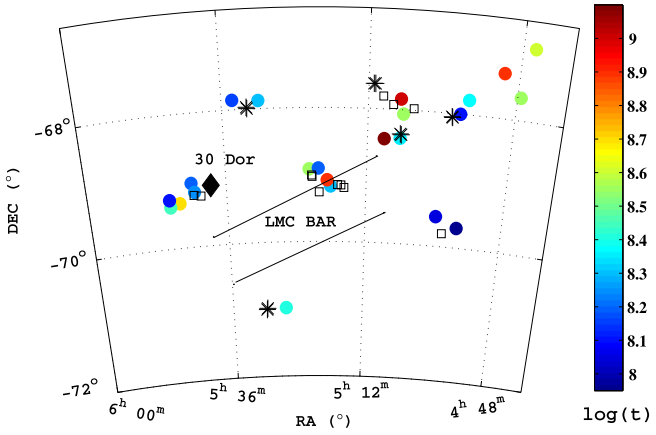

Figure 3. Spatial distribution of 45 studied clusters in the LMC: color-coded circles denote the 23 true single clusters. Black asterisks denote the location of 5 pairs of double cluster, and the black open boxes denote the location of 12 possible clusters/asterisms. The 30 Doradus (black diamond) and the LMC bar (parallel lines) are also shown.

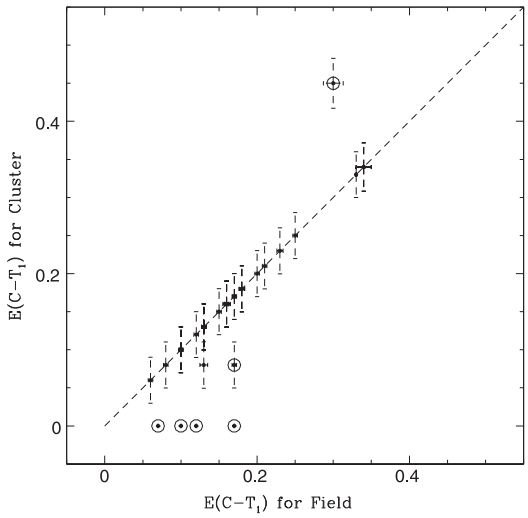

Figure 4. Correlation between estimated cluster and field-reddening values for 33 true clusters. The dashed line corresponds to the one-to-one relation. The deviations are marked with open circles.

features. The estimated ages are compared with these previous estimates in the respective tables. The age comparison shows some agreement with our results, as well as deviation. This is discussed in the next section.

5. DISCUSSION

We have presented a study of 45 inconspicuous, poorly studied clusters in the LMC, based on deep Washington photometry. The data for all of the 45 clusters in the Washington photometric system are presented/analyzed for the first time, and the data have enough photometric depth to identify the turn-off of faint, poorly populated clusters. The data also cover a substantial field region around the cluster to effectively remove the field contamination even in regions with varying density and reddening. The coverage, as well as the depth of the data, has also helped in the identification of possible asterisms and cluster candidates from the sample. We were able to estimate the basic parameters for 33 clusters, out of which 23 are identified as single clusters and 10 are found to

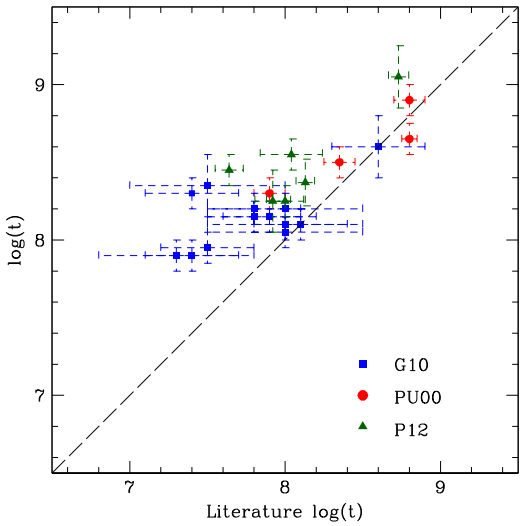

Figure 5. Correlation between derived and published ages by G10, PU00, and P12 for 23 out of the 33 true clusters. For values in G10 we have used the upper limit of the errors. For values of P12 we have used the mean of the upper and lower limit of the errors. The dashed line corresponds to the one-to-one relation.

be members of double clusters. We suggest that the rest of the 12 clusters studied here are possible cluster candidates or asterisms. Out of the 33, 10 true clusters are previously unstudied, and thus we report their sizes, reddenings, and ages for the first time. The rest of the 23 clusters have been previously studied (by either PU00, G10, or P12), but our data are deep enough to derive accurate ages.

The spatial distribution of all of the 45 clusters studied is shown in Figure 3. The 23 true single clusters are represented by color-coded filled circles according to their ages, whereas the 5 double clusters and the 12 cases of possible clusters/asterisms are depicted by black asterisks and black open squares, respectively. The studied clusters are seen to be located mostly in the inner LMC, with a few of them located toward the northwest side. The figure also shows the location of the bar and 30 Dor. For clusters lying in and near such crowded regions, there could be issues due to differential reddening, as well as varying field density. While performing the field star removal from the CMD, we have taken care to choose the field regions carefully, so as to minimize the effects of variation in density and reddening. This has helped in extracting the cluster features in the cluster CMD and the derivation of cluster parameters efficiently.

The RDP method is used to estimate the radius of most of the clusters. In the case of a few clusters, either the RDP did not show a strong peak, or we were unable to derive the RDP due to incompleteness of bright stars near the cluster center, and the cluster radii were chosen as the ones at which the cluster features prominently show up. We have compared the present estimation of radii for 33 true clusters with their previous estimations cataloged by B08, and we find the estimation to be comparable. B08 gives the dimensions of the major and minor axes for these objects, with which dimensions we calculated their mean radius. It is seen that the clusters analyzed are typically small angular-sized objects with radii in the range of $10''$–$40''$ (~2–10 pc). We also find similarity in size for objects under the category of single clusters and double clusters. All of the clusters studied here are small in size and are similar to the sizes of open clusters in our Galaxy. Thus this study helps to derive the parameters of open cluster-like objects in the LMC.

As mentioned earlier, the reddening values for the clusters were adopted from the reddening map of the field region (Subramaniam & Subramanian 2010). We find that the average separation of clusters studied here from the nearest field region is about 6 arcmin. Although this adopted reddening was found satisfactory for most of the clusters, for a few cases the isochrones had to be further reddened/dereddened with respect to the field-reddening values in order to get a proper visual fit of the isochrone. Figure 4 shows a comparison between the reddening values of 33 true clusters and their corresponding fields. The errors in the estimation of the field reddening, taken from Subramaniam & Subramanian (2010), and the error in the reddening of the cluster (photometric error and field-reddening error) are shown in the X and Y axes, respectively. The range of reddening values for the clusters studied is about 0.05–0.45 mag. The cluster reddening is found to be very similar to the field reddening, except for six clusters (marked by open circles). Out of these six cases, four clusters have zero reddening (BSDL 77, BSDL 631, LW 54, and HS 329), and we have not indicated any error bar for them in the figure. H88-52 has less reddening compared to the corresponding field. The cluster HS 390 has the largest value of reddening in our sample and is found to be located near the 30 Dor region. The observed difference in reddening for these six clusters may be due to the spatial variation in reddening and/or the projection effect. The shift in the reddening values of these clusters with respect to the field may cause an additional error in the age estimation. We expect that the error in the age estimation for these clusters can be up to $\Delta\log(t) \sim 0.20$.

We studied the parameters of five double clusters listed in Table 2. A large number of double clusters in the LMC are identified by Dieball et al. (2002). These five pairs are also found to be mentioned in their catalog. The sizes of the double clusters are found to be similar to the single clusters. We expect the reddening and age to be similar among the cluster members in order for the double clusters to be a candidate for a binary pair. For two of the cluster pairs (BSDL 341 and H88-52; KMHK 979 and HS 329) we find that the estimated reddening differs significantly. These clusters also have a fairly large difference in age. The above two differences suggest that these clusters may be pairs because of projection. Two cluster pairs (HS 154 and HS 156; SL 230 and SL 229) have similar reddening, but the ages are not similar, suggesting that they might not be physical pairs. The cluster pair SL 551 and BRHT 38b have comparable reddening and age, within errors. Thus, these two clusters may be a candidate for a binary pair.

The ages of 23 true clusters are compared with the results of PU00, G10, and P12 in Figure 5. Out of 33 true clusters, 13 clusters are in common with G10, whereas six clusters are in common with PU00. A couple of clusters in our sample (BSDL 631 and SL 230) have been studied by both G10 and PU00. For BSDL 631, PU00 estimated an age of $\log(t) < 6.70$ (with no error) and G10 as $\log(t) = 7.50$ ($0.30 \leqslant$ error <0.50). In the case of SL 230, the age estimation by PU00 ($\log(t) = 7.30 \pm 0.05$) and G10 ($\log(t) = 7.40$, with error <0.30) agrees very well within their errors. For both of these clusters we considered the results by G10 for comparison, as it is more recent and the errors are appropriate for such poor clusters. The figure shows that the G10 clusters are primarily younger than $\log(t) \sim 8.50$. P12 used integrated photometry to obtain the

ages of LMC star clusters, and 16 out of 33 true clusters are common with their study. Out of these 16 clusters, G10 has mentioned ages for 8 (BRHT 45a, BSDL 268, H88-320, KMHK 975, NGC 1793, SL 397, SL 579, and SL 551), whereas PU00 has mentioned ages for 2 (H88-265 and H88-269) clusters. Integrated light provides information about the combined stellar population along the line of sight. The clusters studied here are small angular-sized objects embedded within a relatively denser field. Use of integrated photometry to estimate ages for such cases can produce poor results due to field star contamination, stochastic effects, and relatively shallower photometric depth. Thus for comparison we have adopted the age estimates given by G10 and PU00 wherever available, as their results are more reliable, and we considered only six clusters whose ages are given by integrated photometry and finds mentioned only in P12. The comparison suggests that the present study estimates relatively older ages for clusters younger than $\log(t) \sim 7.50$. In the case of young clusters, there is a possibility that our data have missed out brighter stars, and this might cause the above anomaly. The ages of the older clusters are comparable. When we compared our age estimates with those of P12 for 16 clusters, we found that most of the common clusters are younger than $\log(t) = 8.00$. P12 estimated relatively younger ages compared to our estimates for these clusters. We have only a few older clusters, and we find that P12 estimated significantly younger ages for these clusters.

The clusters studied here are of the age up to 1 Gyr, and most of them are poor and inconspicuous clusters. We have also suggested that some of the clusters could be asterisms and not true clusters. The estimates of the radial extent (2–10 pc) of these clusters suggest that they are similar to the open clusters in our Galaxy. We simulated CMDs of a few rich and young clusters using Marigo et al. (2008) isochrones. Assuming the Salpter's mass function and incorporating observational error, we simulated CMDs for the mass range 10–0.5 $M_{\odot}$. The total mass simulated is adjusted to create the same number of stars within 3 mag below the turn-off, as in the observed CMD, after incorporating the Poisson error. This is expected to reduce the effect of incompleteness of fainter stars in the CMD. The estimated masses were found to be up to 1000 $M_{\odot}$ for rich clusters. This is also found to be comparable to the mass estimates of P12 for the same clusters. Adopting the masses of all common clusters from P12, the relatively rich clusters in our sample are up to 1000 $M_{\odot}$, whereas the poor clusters are only a few 100 $M_{\odot}$. Thus, the masses also suggest that these clusters are similar to the open clusters of our Galaxy. We also find that the mass limit at which the object is unable to be identified as a cluster is about a few 100 $M_{\odot}$. At this mass limit, the number of stars formed are unable to create either a notable density enhancement, an identifiable cluster sequence in the CMD, or both.

Baumgardt et al. (2013) have studied the star cluster formation history of the LMC, using some recent catalogs that include PU00, G10, and P12. Their Figure 3 shows a plot between the mass and age of all of the clusters. The mass of the clusters ranges from a few hundred to a few thousand of $M_{\odot}$ and are within the age range 10 Myr to 1 Gyr. The figure shows that the number of clusters at the higher end of the mass distribution is relatively greater compared to the lower end, where the contribution is primarily from G10. However, the age limit for G10 clusters is constrained only to $\leqslant$ 300 Myr. The estimated mass range of our studied sample contributes to this lower end of the cluster mass distribution and also contains clusters beyond the age limit of G10. As mentioned earlier, a significant fraction of our clusters lie within the age range of (100–300) Myr which corresponds to the recent star formation in the last 200 Myr. This suggests that the LMC has produced very low mass clusters, along with the massive and rich clusters in the recent past. Thus, in the context of understanding the cluster mass function in the LMC, our study has added many clusters to the lower mass limit of the distribution. The poor clusters are also of interest to understand the survival time of these clusters in the LMC. Table 3 suggests that the possible clusters/asterisms are in the age range of $\log(t) = 8.10$–8.80, probably suggesting their survival time. This timescale is also similar to that in our Galaxy (a few 100 Myr; Bonatto et al. 2010).

6. SUMMARY

1. The study is aimed to enlarge the number of objects confirmed as genuine star clusters and to estimate their fundamental parameters. We present Washington photometry of 45 star clusters distributed in the inner LMC, some of which are projected toward relatively crowded fields.
2. Out of the 45 clusters, 33 are found to be true (genuine) cluster candidates, whereas the remaining 12 clusters could only be categorized as possible clusters/asterisms. We successfully estimated the parameters of the true clusters and at the same time listed the parameters of the other category, if they are clusters at all. The age distribution of the true clusters shows that about 50% fall within the age range (100–300) Myr, whereas some are older or younger.
3. The physical sizes and masses of the studied clusters are found to be similar to that of open clusters in the Milky Way. Our study adds to the lower end of the cluster mass distribution in the LMC. Thus the LMC, apart from hosting rich clusters, also contains such small, less massive open clusters, particularly in the (100–300) Myr range.
4. The 12 poor cases in the category of possible clusters/asterisms are also worthy of attention, in the sense that they can throw light on the survival time of such objects in the LMC.

APPENDIX A
SINGLE CLUSTERS

Notes on single clusters are presented here. Multipanel plots corresponding to each cluster are shown in Figure A1 (BRHT 45a, BSDL 77, H88-33, H88-131, H88-320, and H88-331), Figure A2 (HS 116, HS 131, HS 390, HS 411, HS 412, and KMHK 95), and Figure A3 (KMHK 907, KMHK 975, LW 54, and SL 579).

1. BRHT 45a is a bright, young (~125 Myr) cluster with prominent upper MS and MSTO. Dieball et al. (2002) reports a second cluster BRHT 45b at coordinates (4^{h} 56^{m} 52^{s}, -68° $00'$ $20''$), which lies within the cluster radius ($27''$) of BRHT 45a. G10 mentions that BRHT 45b is a young cluster aged ~40 Myr ($\log(t) = 7.60$, with $0.30 \leqslant$ error <0.50), which is similar to the age estimated by P12 using integrated photometry ($\log(t) = 7.62^{+0.18}_{-0.32}$). We in

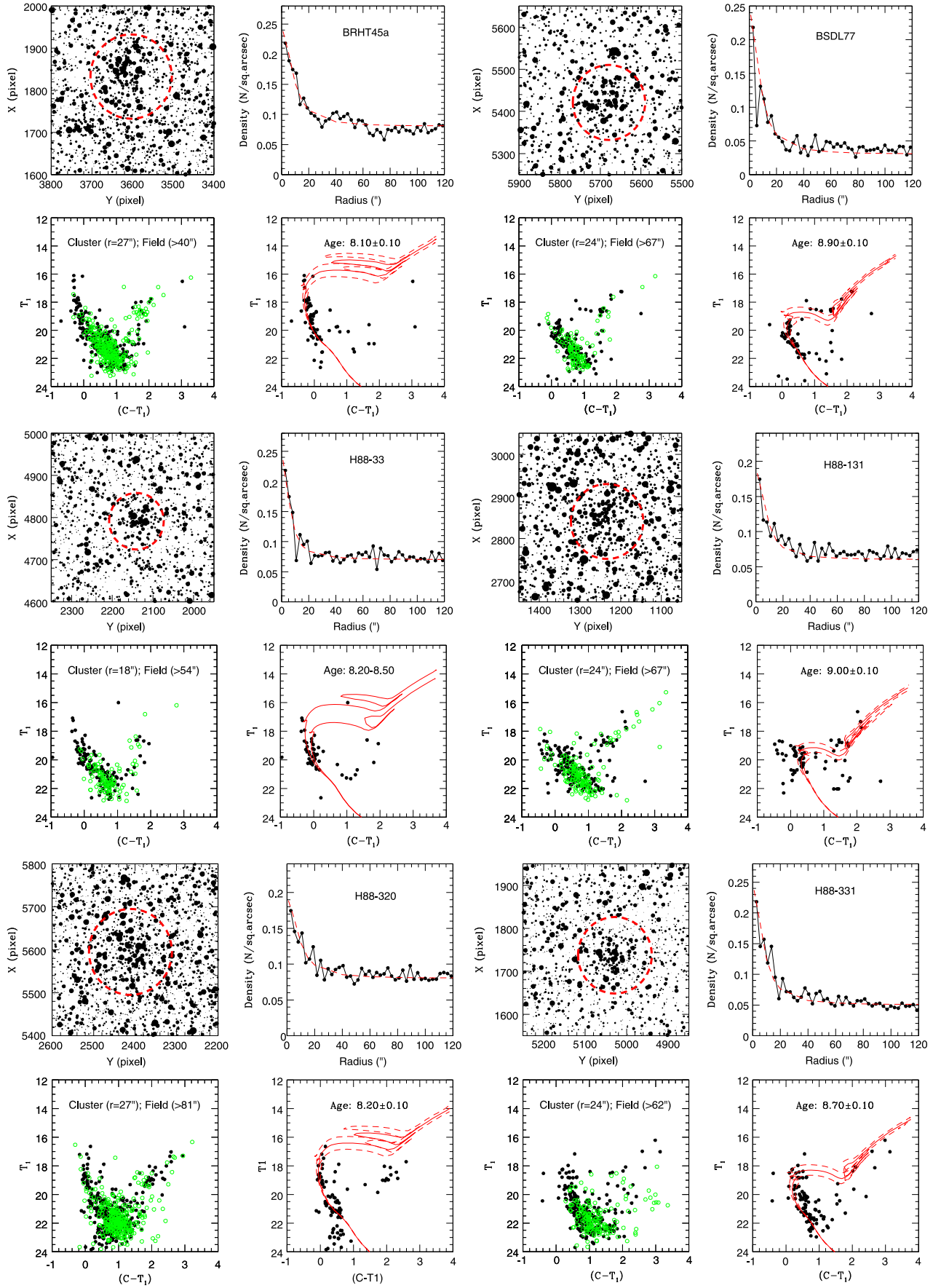

Figure A1. Single-cluster candidates: BRHT 45a, BSDL 77, H88-33, H88-131, H88-320, and H88-331. Panel description for each cluster is the same as for Figure 1.

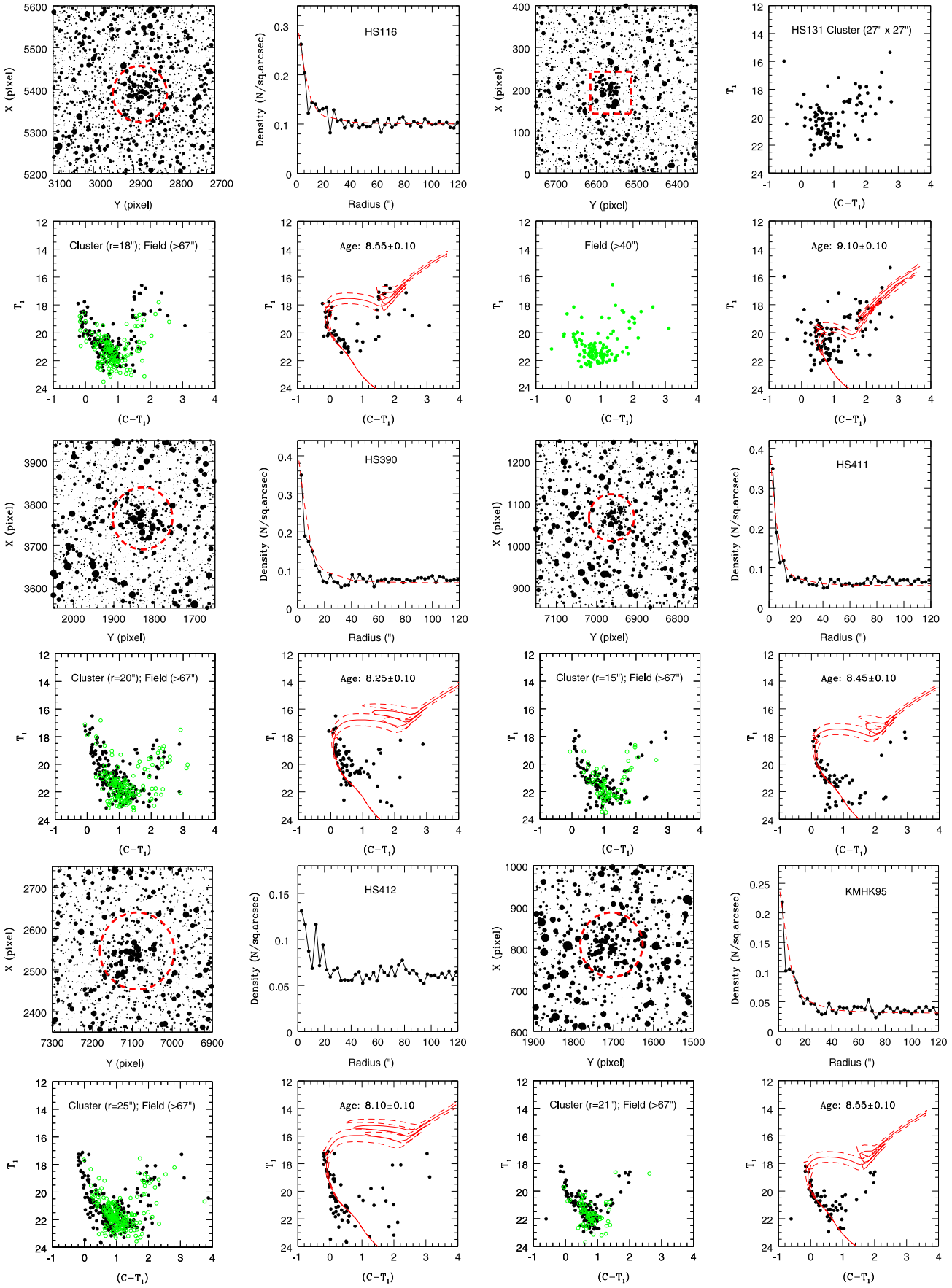

Figure A2. Single-cluster candidates: For HS 116, HS 390, HS 411, HS 412, and KMHK 95, the panel description for each cluster is the same as for Figure 1, except that in the case of HS 412, no King profile overplot to RDP is shown. For HS 131, the top right panel shows the CMD of stars within the estimated cluster size (black filled circles). The bottom left panel shows the CMD of the annular field (green filled circles), whereas the bottom right panel shows isochrones overplotted to the unclean cluster CMD. The top left panel description for HS 131 is the same as for Figure 1.

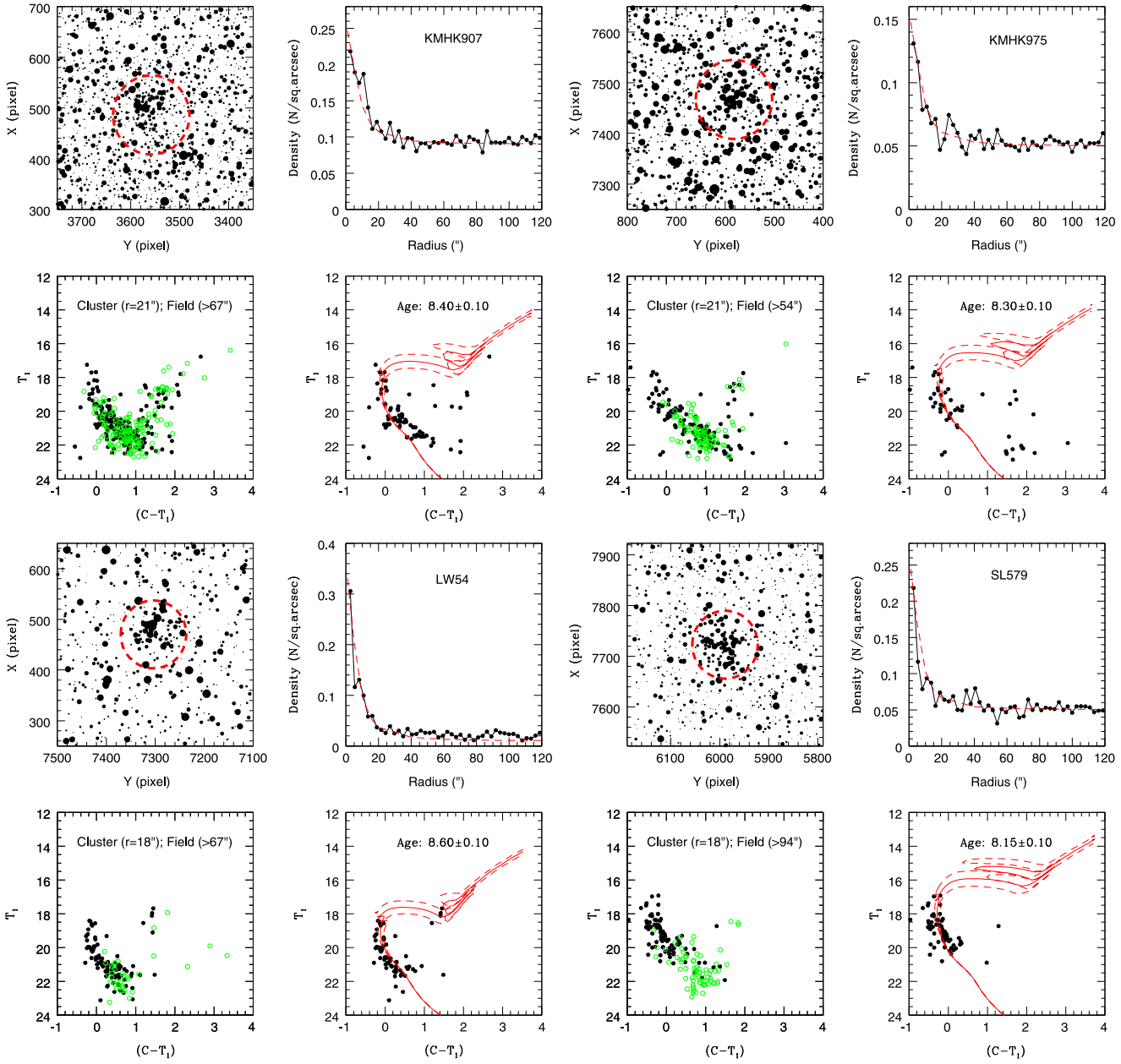

Figure A3. Single-cluster candidates: KMHK 907, KMHK 975, LW 54, and SL 579. Panel description for each cluster is the same as for Figure 1.

fact identified three clumps of stars within the cluster region, and one of them could possibly be BRHT 45b. Piatti (2014) considered only the central clump as BRHT 45b and estimated the age as ∼80 Myr ($\log(t) = 7.90 \pm 0.10$). However, given such a small spatial separation, it is difficult for us to identify BRHT 45a and BRHT 45b separately and estimate independent parameters for them. The age we have determined is possibly the age of the youngest or the dominant clump.

2. BSDL 77 is a compact cluster (aged ∼800 Myr) with a prominent MS, MSTO, and a red giant branch. We also notice a clumpy distribution of stars in the cluster region, which is reflected in the RDP. This is one of the older clusters studied here.
3. H88-33 is a small compact cluster. The MSTO shows two possible turn-offs. As the cluster MS is very well populated, the scatter near the MSTO may be due to statistical effects. We have shown isochrones of $\log(t) = 8.20$–8.50, suggesting that the age of the cluster is likely to be in this range.
4. H88-131 is a moderately large cluster, as shown by the RDP. The field-subtracted CMD shows a MS with a number of stars bluer than the MSTO. A few red giants can also be identified in the CMD. We have estimated the age of the cluster to be $\log(t) \sim 1$ Gyr. As the reddening to the cluster is very small, the stars seen to be bluer than the MS demand attention.
5. H88-320 is a fairly large cluster located in a relatively dense field, as shown by the RDP. The cluster MS is clearly identified in the field-subtracted CMD, and the age is estimated to be ∼160 Myr.
6. H88-331 is a dense and rich cluster. The MS has relatively large width, and the MSTO also shows scatter. This may be due to the presence of differential reddening

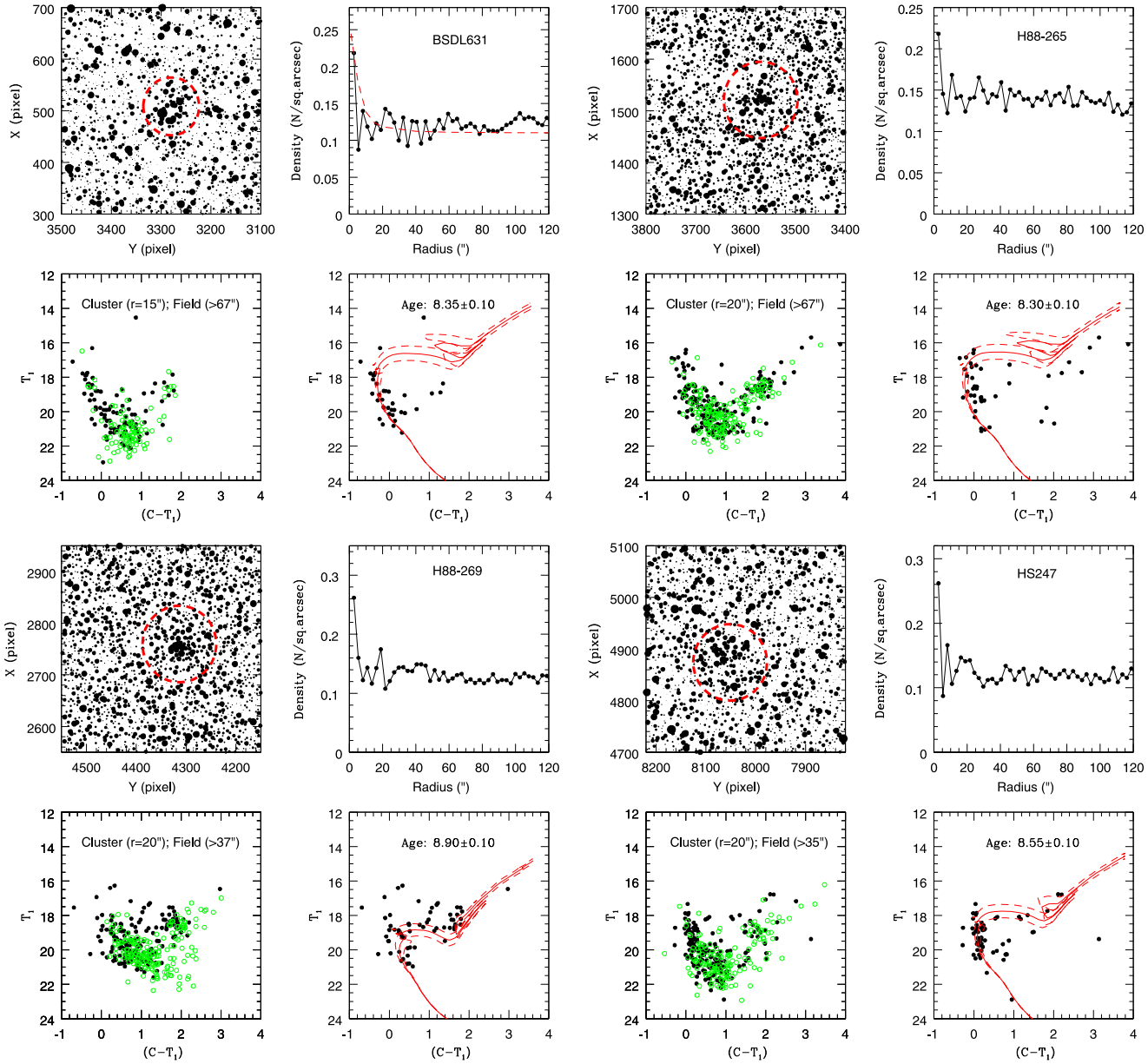

Figure A4. Single clusters with weak RDP: BSDL 631, H88-265, H88-269, and HS 247. Panel description for each cluster is the same as for Figure 1, except that no King profile overplot to RDP is shown for H88-265, H88-269, and HS 247.

in the field. The age estimated for this cluster is ∼500 Myr.

7. HS 116 is a small cluster in a relatively dense field. The field-subtracted CMD shows the cluster features well, which can be visually fitted with isochrones aged ∼350 Myr.
8. HS 131 is a dense rich cluster easily identified in the field. The RDP does not allow us to define the cluster radius, and the features in the CMD also show large scatter. A spatial plot of the evolved stars showed a density enhancement near the cluster center, and we estimated the extent of the cluster to be about ($27'' \times 27''$) around the cluster center. We thus considered all stars within this region, and the age of the cluster was estimated using a visual fit of the isochrones, especially to the RC and the RGB stars as ∼1.25 Gyr.
9. HS 390 is a dense and slightly elongated cluster with a well populated MS and no giants. The estimated age is ∼180 Myr.
10. HS 411 is one of the small clusters where we could identify a narrow and well-populated MS. The cluster is aged ∼280 Myr.
11. HS 412 shows clumpy distribution of stars in the cluster region, giving rise to RDP with multiple peaks. The cluster MS is prominent, and we estimate the age to be ∼125 Myr.
12. KMHK 95 is a moderately rich cluster with a well-defined cluster MS. The cluster MS is clearly identified in the field-subtracted CMD to estimate the age (∼350 Myr).
13. KMHK 907 is a bright, young cluster whose upper MS is prominently visible, and its age is ∼250 Myr. The lower portion of the MS is broadened, and the width increases with decrease in magnitude. This feature stays even after

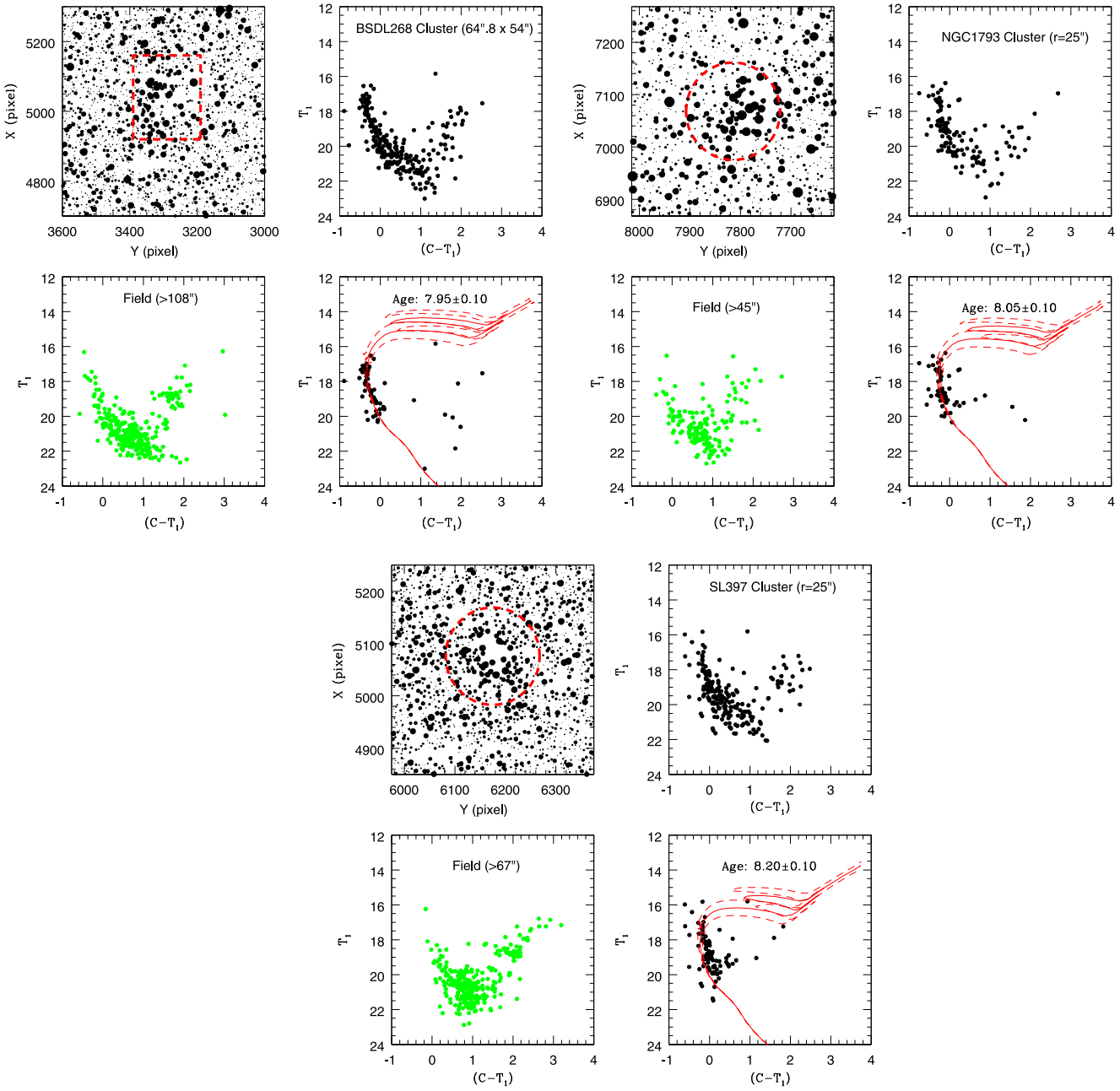

Figure A5. Single-cluster candidates with no RDP: BSDL 268, NGC 1793, and SL 397. For each of these cases, the top right panel shows the CMD of stars within the estimated cluster radius (black filled circles), whereas their bottom left panel shows the CMD of the annular field (green filled circles). The top left and bottom right panel descriptions for these clusters are the same as for Figure 1.

cleaning with field regions at different annular radii. This is possibly an effect of differential reddening or the presence of equal mass binaries in the lower MS, which can be visually fitted by brightening the isochrones by 0.75 mag. Dieball et al. (2002) mentions the presence of another cluster in this field, BSDL 1716, with coordinates (5^h 26^m 07^s, -70° $59'$ $19''$) and of similar size as KMHK 907. B08 lists BSDL 1716 as an association. We find no information about the age of BSDL 1716 from PU00 or G10. Given its coordinates, it is possible that the bright clump seen in the spatial plot toward the southwest direction (at a distance of $\sim 33''$) of KMHK 907 is BSDL 1716. However, we could not find any prominent cluster feature in that specific location, and hence we are unable to derive any cluster parameters for the same.

14. KMHK 975 is a small cluster where the CMD of the cluster region before field star subtraction shows a broad MS and a few RGs. The field-subtracted CMD has only the upper part of the MS, as the lower part has been subtracted away, even though the limiting magnitude of this region is about $T_1 \sim 23$ mag. The age estimated using the upper MS is ~200 Myr.
15. LW 54 is a compact and dense cluster that shows two concentrations of stars in the cluster region. The field region is very sparse, as shown by the RDP. The cluster features are clearly seen in the CMD and are used to estimate the age (~400 Myr).

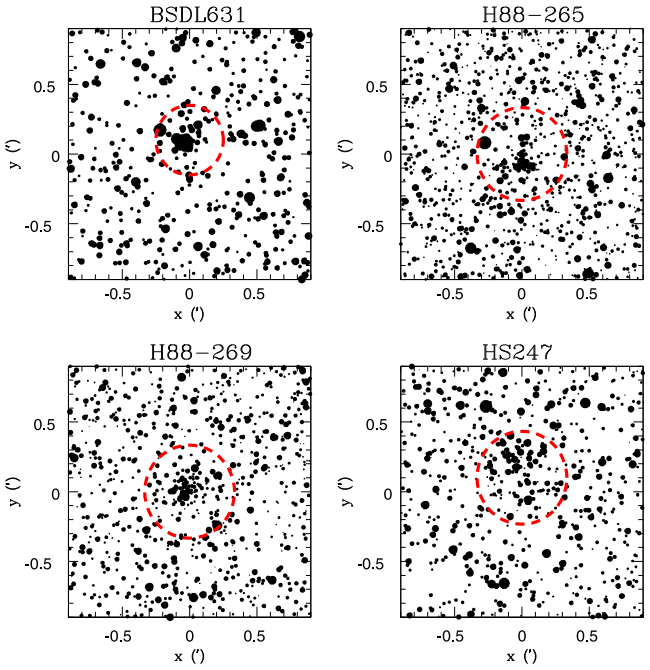

Figure A6. OGLE III fields of clusters with weak RDP: BSDL 631, H88-265, H88-269, and HS 247. The red dashed circle shows the derived size for these clusters using our Washington data.

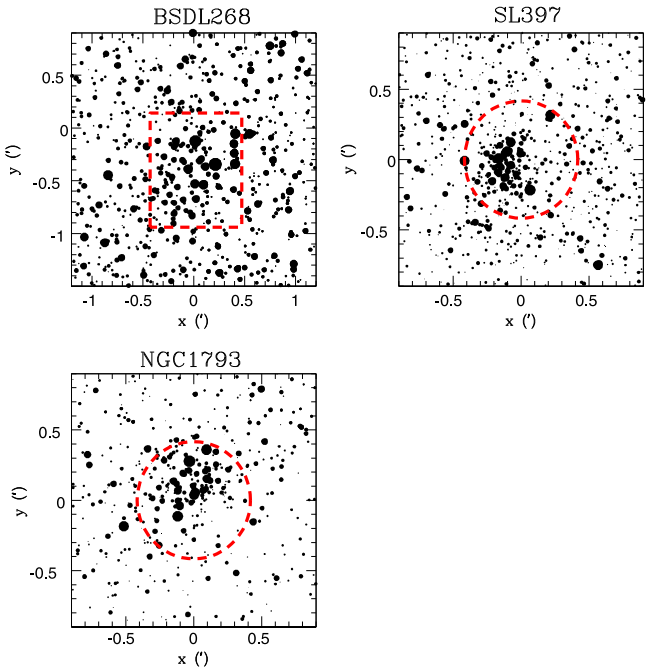

Figure A7. OGLE III fields of clusters with no RDP: BSDL 268, NGC 1793, and SL 397. The red dashed circle/rectangle shows the derived size for these clusters using our Washington data.

16. SL 579 is a rich and dense cluster. The CMD of the region is relatively shallow, with a limiting magnitude of $T_1 \sim 21$ mag. The cleaned CMD has a well-populated MS, which is used to derive the age (∼140 Myr).

We discuss below the cases of some clusters for which either the RDP did not show a strong peak (BSDL 631, H88-265, H88-269, and HS 247 in Figure A4) or where we could not obtain an RDP (BSDL 268, NGC 1793, and HS 329 in Figure A5). Saturation effects caused by the presence bright stars near the cluster center have resulted in missing stars and incompleteness in the central region for these clusters. As our data could not confirm whether these clusters are true clusters based on spatial density enhancement, we tried to verify the existence of these clusters by identifying density enhancement using other optical data. The OGLE III is one of the complete and relatively deep surveys of the inner region of the LMC (4°–5°) with good spatial resolution (Udalski et al. 2008). We extracted the OGLE III fields corresponding to each of these clusters and created similar finding charts (Figure A6 for BSDL 631, H88-265, H88-269, and HS 247; and Figure A7 for BSDL 268, NGC 1793, and HS 329). It is to be noted that in the OGLE III spatial plots presented in this section and hereafter (i.e., for a few cases in Appendices B and C), x and y denote the Cartesian coordinate system (units in arcminutes), with north on top and east to the left. The individual cases are discussed below.

1. BSDL 631: a small, compact cluster with symmetric distribution of bright stars is observed around the cluster center. The estimated RDP shows only a weak density enhancement within a radius $\leqslant 15''$ mainly due to missing stars near the center. The OGLE III field compliments the Washington field, showing a small but compact clump of bright stars present within the cluster region, and is devoid of saturation effects. Based on the density enhancement seen in the OGLE III field (Figure A6) and the MS feature identified in the CMD, we conclude that BSDL 631 is a very small, compact, and young cluster, aged ∼220 Myr.
2. H88-265: a small but prominent clump of stars is observed around the cluster center in the spatial plot. A comparison of the CMD of the cluster region with the field region shows prominent MSTO and upper MS features (brighter than 19.0 mag and bluer than 0.2 mag), which could belong to the cluster. A spatial distribution of the bright stars shows significant clumping around the cluster center within a radius, $r \leqslant 20''$ and is hence adopted as the cluster radius. The OGLE III spatial plot (Figure A6) corresponding to H88-265 shows a similar small but prominent clump of bright stars around the cluster center, thus validating the presence of this small and young cluster, aged ∼200 Myr.
3. H88-269: the finding chart shows a small, dense clump of stars near the central region. The density enhancement observed is caused by stars near the MSTO, as well as evolved stars, as seen in the cleaned cluster profile. The cluster CMD can be visually fitted with an isochrone of age $\log(t) = 8.90 \pm 0.10$. Although the RDP estimated for this cluster does not show a strong peak, we find the cluster profile to prominently show up within a radius of $20''$. In fact, the field seems to be have almost similar SFH to that of the cluster and suffers from differential reddening, thus making field star subtraction inefficient. To verify the existence of this cluster, we extracted the OGLE III field (Figure A6) for this cluster and were able to find a very significant density distribution of stars within the central region. We conclude that H88-269 is a small and compact cluster, aged ∼800 Myr, immersed in a dense field of almost similar age.
4. HS 247: we observe feeble density enhancement near the expected center of the cluster. However, a strong upper MS (brighter than 20.0 mag and bluer than 0.4 mag) is

observed when the CMDs of the cluster and the field region are compared. This prominent cluster feature is retained even after cleaning with alternate field regions. A spatial distribution of these bright stars shows significant density distribution around the cluster center. The cluster radius (20″) is selected as the radius at which the cluster profile looks well-populated. The OGLE III spatial plot (Figure A6) corresponding to HS 247 shows a density enhancement within the cluster region, supporting the existence of this cluster. We suggest that HS 247 is a small, young cluster, aged ∼350 Myr.

5. BSDL 268: this is one of the youngest clusters in our sample, aged ∼90 Myr. In the spatial plot we see a few bright stars clumped near the expected cluster center, with evidence of some missing stars. A comparison of the CMDs of the cluster and field region shows a bright upper MS, brighter than 19.0 mag and bluer than 0.2 mag. Also, the cleaned CMD has a well-populated MS. A spatial plot of these bright MS stars shows a compact distribution within an area of about (64.″8 × 54″), and the cluster center is chosen at the center of this distribution. The corresponding OGLE III spatial plot (Figure A7) for the cluster shows strong density enhancement due to bright stars in the central region validating this young cluster candidate.
6. NGC 1793: we considered an area of (54″ × 54″) around the central region where the presence of a cluster is suspected. The CMD shows a strong upper MS brighter than 19.0 mag and bluer than 0.2 mag, which could belong to the cluster, and SFH appears quite different from that of the field CMD. A radius of 25″ is selected for the cluster, and the cluster feature is found to appear clearly in the cleaned CMD. The corresponding OGLE III spatial plot (Figure A7) for the cluster is presented, which shows a strong density enhancement due to bright stars in the central region validating this to be a true cluster, aged ∼110 Myr.
7. SL 397: the spatial plot shows a clumpy distribution of bright stars located symmetrically around the expected cluster center and possibly some missing stars. The bright stars form a prominent upper MS (brighter than 19.0 mag and bluer than 0.2 mag) for the cluster, even after cleaning the field stars. We were unable to estimate an RDP. The cluster radius (25″) is selected as the distance from the center at which the cluster features seem to be well-populated. The corresponding OGLE III spatial plot (Figure A7) for the cluster shows a strong density enhancement in the central region. This further confirms the object as a true young (∼160 Myr) cluster.

APPENDIX B
DOUBLE CLUSTERS

In this section, we discuss the cases of double clusters. Their corresponding multipanel plots are shown in Figure B1 (BSDL 341 and H88-52; HS 154 and HS 156; KMHK 979 and HS 329) and Figure B2 (SL 230 and SL 229; SL 551 and BRHT 38b). The OGLE III spatial plot corresponding to KMHK 979 is presented in Figure B3.

1. BSDL 341 and H88-52: these are a pair of young and intermediate-age clusters, with their centers separated by ∼60″. BSDL 341 is the younger (∼280 Myr) of the pair, showing a bright upper MS. H88-52 is an intermediate-age (∼1.1 Gyr) and compact cluster, showing prominent MSTO and RC stars, located in the bottom southwest direction of BSDL 341.
2. HS 154 and HS 156: these are two clusters, with their centers separated by ∼81″. HS 154 is the young (∼450 Myr, i.e., $\log(t) = 8.65 \pm 0.10$), cluster, with a prominent upper MS. Piatti (2012) has studied this cluster and estimated an age of $\log(t) = 8.70 \pm 0.10$. HS 156 is an intermediate-age (∼1.1 Gyr) cluster, showing a prominent MSTO, located in the eastern direction of HS 154. Palma et al. (2013) and Piatti (2014) both found HS 156 to be an intermediate-age cluster, aged ∼1 Gyr. In this study we looked upon HS 154 and HS 156 from the point of view of a double cluster. Also, we find excellent agreement of our derived ages for both of these clusters when compared with their respective previous studies.
3. KMHK 979 and HS 329: KMHK 979 is a young cluster, aged ∼80 Myr. We are unable to estimate an RDP for this cluster. We choose the cluster radius (20″) at which the cluster profile becomes well-populated. Due to the proximity of clusters in the field, we choose fields of similar dimension in different parts of the observed field, away from the cluster, to clean the cluster profile. The cluster may be younger than our estimated age due to missing bright stars at the center. We have extracted the corresponding OGLE III field for this cluster (Figure B3). The OGLE field shows clear density enhancement due to bright stars at the center of KMHK 979, thus validating the existence of a true young cluster.

   The second member of the pair, HS 329, is identified as a dense clump of stars distributed asymmetrically at ∼68″ away toward the southeast direction of KMHK 979. The CMD of this clumpy region shows the existence of an evolved population such as RC and RGB stars, along with a spread in MSTO. An eye-estimated center in the clumpy region is chosen as the cluster center, and we estimate that the cluster is spread across an area of (37.″8 × 40.″5) around this center, based on the clumpy distribution of the evolved stars. The CMD of the field region also shows the presence of evolved stars. In addition, the whole field suffers from high differential reddening, owing to its location near the central region of the LMC, thus making it inconvenient to identify the cluster MSTO efficiently after cleaning. Due to insufficient coverage of the field region on the southern side of the cluster, we could not perform annular field subtraction. Field star subtraction using fields of similar dimension in different parts of the observed field (away from the cluster) was hence tried out. A unique determination of age for this cluster was found to be difficult, and we suggest that the cluster might be in the age range of 800 Myr to 1 Gyr.

   According to Dieball et al. (2002), there exists a third cluster, BSDL1980, in this field with coordinates (5^h 29^m 33^s, −70° 59′ 38″). The average radius suggested by them is ∼11″, smaller when compared to the sizes of KMHK 979 and HS 329. According to G10, this cluster is a young one (∼20 Myr) and is clearly seen as a small and poorly density enhanced spot in the OGLE III spatial plot (Figure B3) toward the southwest direction of KMHK 979. However, due to the incompleteness of bright stars in

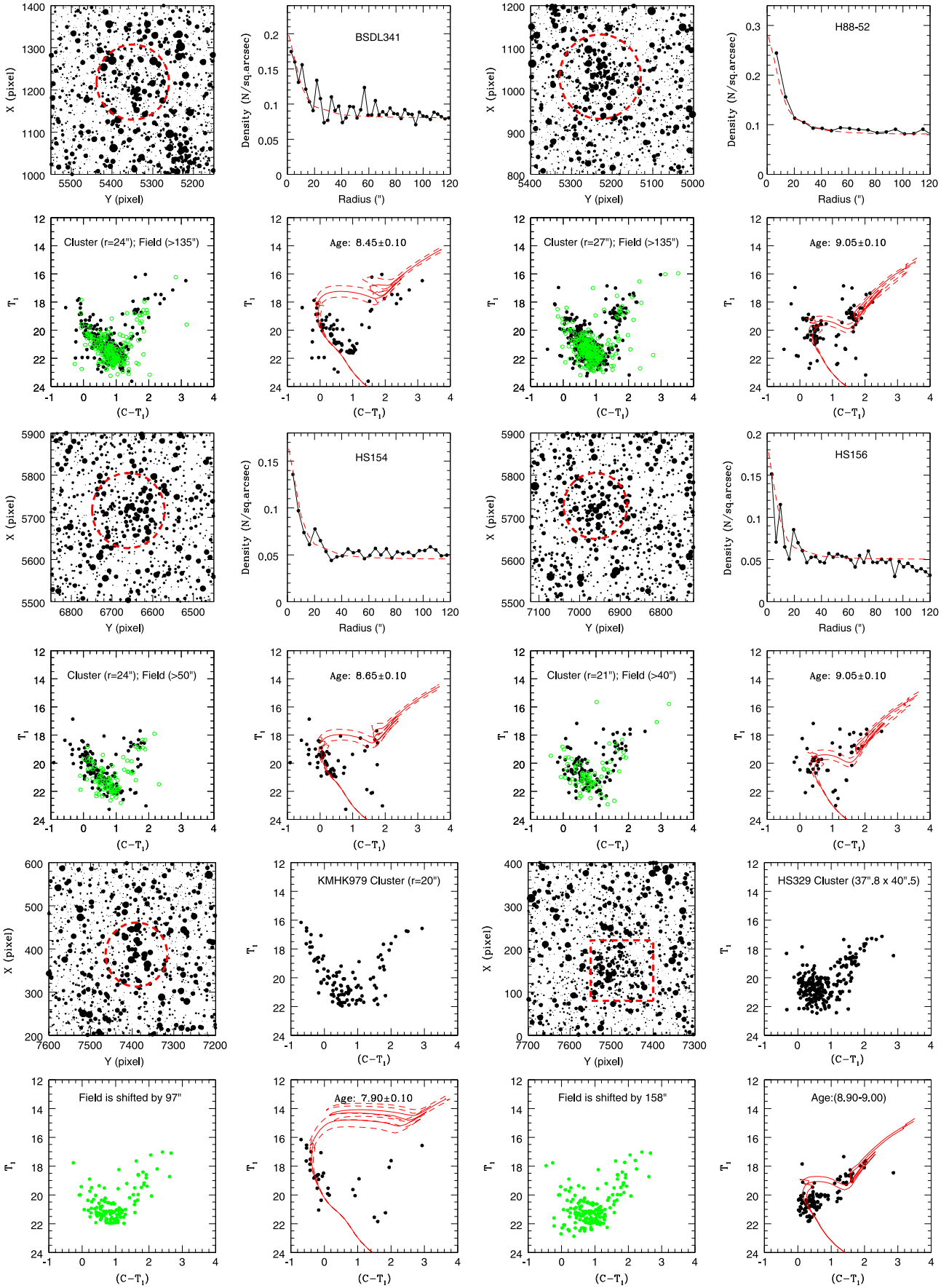

Figure B1. Double clusters: BSDL 341 and H88-52; HS 154 and HS 156; KMHK 979 and HS 329. The panel description for the first two pairs is the same as that of Figure 1. For KMHK 979 and HS 329, the top right panel shows the CMD of stars within the estimated cluster radius (black filled circles), whereas the bottom left panel shows the CMD of a nonannular, similar sized field region (green filled circles) located away from the clusters. The top left and bottom right panel descriptions are the same as for Figure 1.

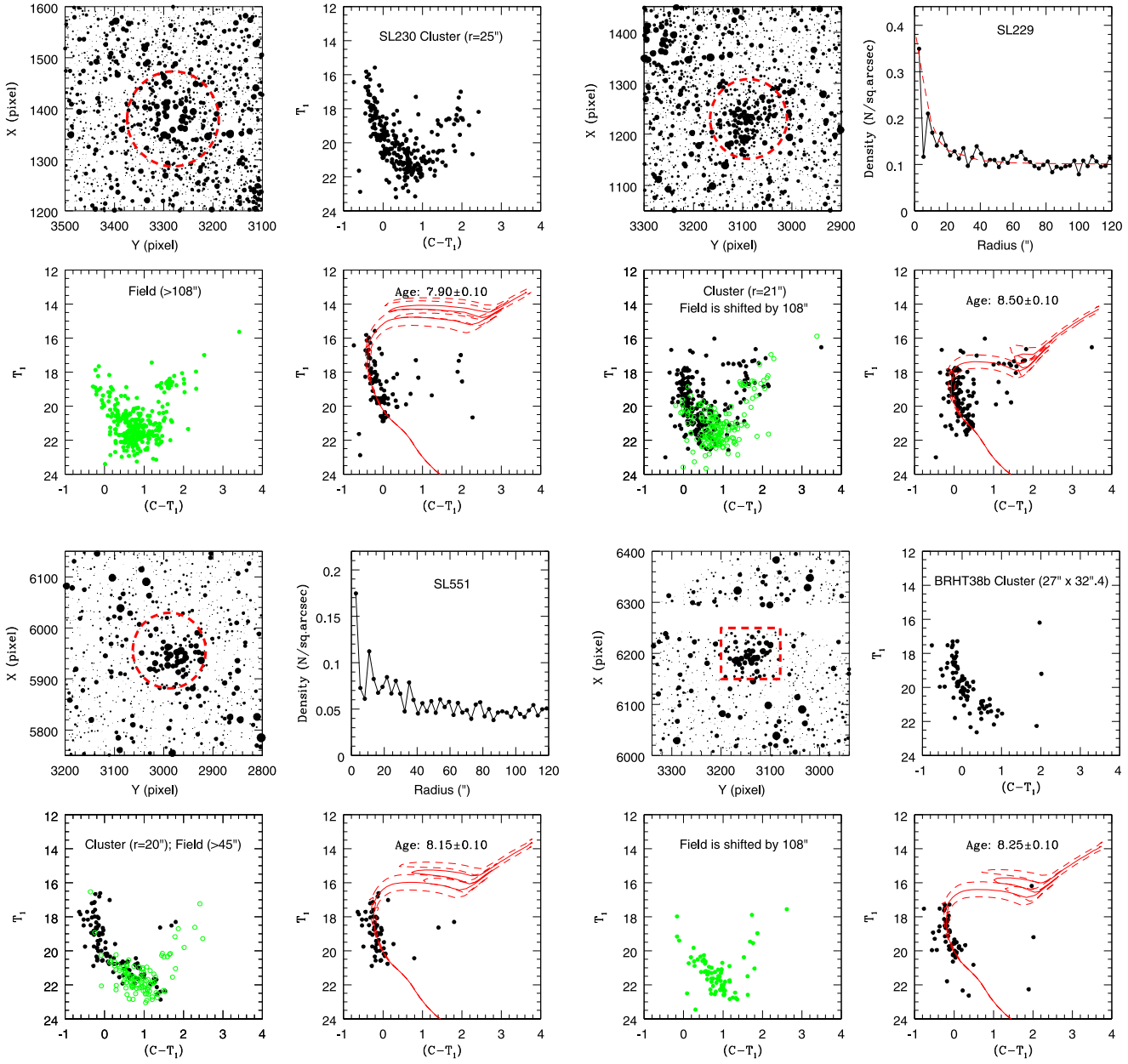

Figure B2. Double clusters: SL 230 and SL 229; SL 551 and BRHT 38b. For SL 229 the field CMD is of a nonannular, similar sized region located away from the cluster. For SL 551, no King profile overplot to RDP is shown. For SL 230 and BRHT 38b the top right panel shows the CMD of stars within the estimated cluster size (black filled circles), whereas the bottom left panel shows the CMD of an annular/nonannular, similar sized field region (green filled circles) located away from the cluster. The top left and bottom right panel descriptions for these clusters are the same as for Figure 1.

our data, we have not been able to estimate the parameters of this cluster.

4. SL 230 and SL 229: these are two young bright clusters with prominent upper MS and MSTOs. The younger cluster, SL 230, is aged ∼80 Myr. Some of the bright stars near the cluster center were saturated, and hence the photometry could not be done. It was difficult to construct an RDP for SL 230. We thus selected the cluster radius ($r = 25''$) as the one at which the cluster features were found to be well-populated. It is quite possible that we missed out some bright members of the cluster due to saturation, and hence SL 230 may be younger than our estimate. SL 229 is located in the southwest direction of SL 230, with its center separated by ∼66″, and is aged around ∼320 Myr. Due to insufficient data coverage in the southern direction for SL 229, we performed field star subtraction using circular fields in different directions away from the cluster. This cluster has been studied by Piatti (2012), and the author's age estimation agrees with ours. We studied these clusters as a double cluster with a first time age estimation of SL 230, using deep Washington photometric data, along with a reconfirmation of the age of SL 229.
5. SL 551 and BRHT 38b: these are two young (∼160 Myr) and bright clusters whose upper MS and MSTO are prominently visible in their respective CMDs. BRHT 38b is located toward the northeast direction of SL 551 within a separation of ∼77″. For BRHT 38b we consider rectangular areas of different dimensions around an eye-estimated center in the clumpy region and for which the

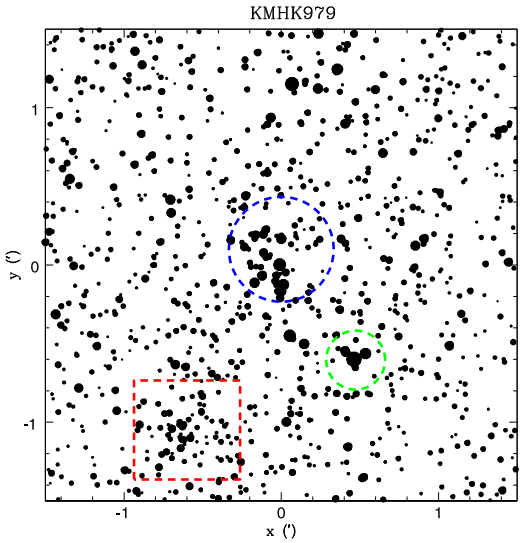

Figure B3. OGLE III field of KMHK 979. The blue dashed circle and red rectangle denote the extent of KMHK 979 and HS 329, respectively, as estimated using our Washington data. The green dashed circle denotes the average size of BSDL1980, estimated from Dieball et al. 2002.

cluster features are well-populated, which gives us the extent of the cluster. Due to insufficient data coverage in the northern direction of BRHT 38b, the cluster CMD is cleaned using rectangular fields of same area located in different parts of the observed field away from the cluster.

APPENDIX C
POSSIBLE CLUSTERS/ASTERISMS

We discuss the individual cases categorized as possible clusters/asterisms below. Their corresponding multipanel plots are shown in Figure C1 (BSDL677, H88-235, H88-244, H88-288, and H88-289), Figure C2 (H88-307, H88-316, KMHK 378, KMHK505, and OGLE 298) and Figure C3 (H88-279 and SL 269). The OGLE III spatial plots corresponding to H88-279 and SL 269 are presented in Figure C4.

1. BSDL677: the center of the cluster field (as mentioned in B08 catalog) is chosen as the cluster center. The estimated RDP shows a feeble density enhancement within a radius of 21″. The CMD of stars within this radius seems to exhibit a poor upper MS (brighter than 19.0 mag and bluer than 0.2 mag), which may belong to the cluster. The upper MS feature becomes unclear after field star subtraction, and visual fitting of isochrones to these few bright stars suggests an age of ∼180 Myr. Based on such feeble density distribution and unclear upper MS, we conclude that BSDL677 is either a very poor cluster or an asterism.
2. H88-235: in the spatial plot, no clear density enhancement is observed near the expected center of the cluster. We estimated the RDP, which supports the same and shows only a very poor density enhancement within 15″. A CMD within this radius shows a few upper MS stars brighter than 20.0 mag and bluer than 0.6 mag that may belong to the cluster. We also find a good number of such stars distributed in the field, suggesting that the field, as well as the cluster, has similar MS, and the field star subtraction renders a very poor cluster MS in the CMD. Visual fitting of isochrones to the poor upper MS suggests an age of ∼560 Myr ($\log(t) = 8.75 \pm 0.20$). Previous study by P12 mentions an age of ∼350 Myr ($\log(t) = 8.55^{+0.02}_{-0.08}$) for this cluster, which moderately agrees with our estimation within the errors. With almost negligible density enhancement, poor cluster features, and similar SFH as the field, H88-235 is likely to be an asterism.
3. H88-244: the spatial plot of H88-244 looks almost homogeneous, with no significant density enhancement near the expected cluster center. The center of the cluster field (as mentioned in B08 catalog) is chosen as the cluster center, and the CMD extracted within the estimated cluster radius (25″) seems to show a very poor upper MS (brighter than 19.0 mag and bluer than 0.4 mag), which may belong to the cluster. However, the spatial distribution of the bright upper MS stars does not show any significant density enhancement at the location of the cluster and looks almost homogeneous. Feeble cluster features, similarity between field and cluster CMDs, as well as a large amount of differential reddening within the field region, makes it inconvenient to efficiently identify the presence of the cluster. The estimated reddening for this cluster is about 0.25 mag, much higher than the reddening of the corresponding field, which is 0.10 mag. If a cluster exists at all, it is a small, poor, and young (∼200 Myr, i.e., $\log(t) = 8.30 \pm 0.20$) one. Previous study by PU00 mentioned an age of ∼125 Myr ($\log(t) = 8.10 \pm 0.10$), which agrees with our estimate within the errors.
4. H88-288 and H88-289: H88-289 is located toward the north of H88-288 at a distance of about 74″. They seem to show poor density enhancement around their respective cluster centers and exhibit a poor upper MS (brighter than 19.0 mag and bluer than 0.4 mag) within their estimated radii. Their size and age (∼250 Myr, i.e., $\log(t) = 8.40 \pm 0.20$) are almost similar. However, H88-289 could be younger than our estimated age, as some bright MSTO/upper MS stars seem to be missing from the central region due to the saturation effect. Using integrated photometry, P12 estimated the ages for H88-288 and H88-289 to be $\log(t) = 8.04^{+0.20}_{-0.04}$ and $\log(t) = 7.80^{+0.43}_{-0.03}$, respectively, which is younger relative to our estimate. We realized that the field region for this pair suffers from variable density and reddening. Hence decontaminating the cluster CMD from field stars was found to be difficult for this pair of clusters. We conclude that with such poor density enhancement and cluster features, along with issues related to variations in density and reddening within the field region, it is difficult to categorize H88-288 and H88-289 as true clusters.
5. H88-307: it is difficult to observe any prominent dense clump of stars within the central region. The cluster and the field regions show similar features in the CMD, thus posing difficulty to efficiently identify the presence of a cluster and estimate its corresponding parameters. The center of the cluster field (as mentioned in B08 catalog) is chosen as the cluster center. A comparison of the cluster and field CMD suggests a very poor upper MS (brighter than 19.0 mag and bluer than 0.4 mag). The cleaned CMD has very few MS stars. If a cluster is present at all, it could be poor and young (∼180 Myr), located within an area of (54″ × 54″) around the cluster center. Dieball et al. (2002) mention the presence of two more clusters within the same field. These are BSDL2768 ($5^h\ 40^m\ 39^s$, $-69^\circ\ 15'\ 29''$) and

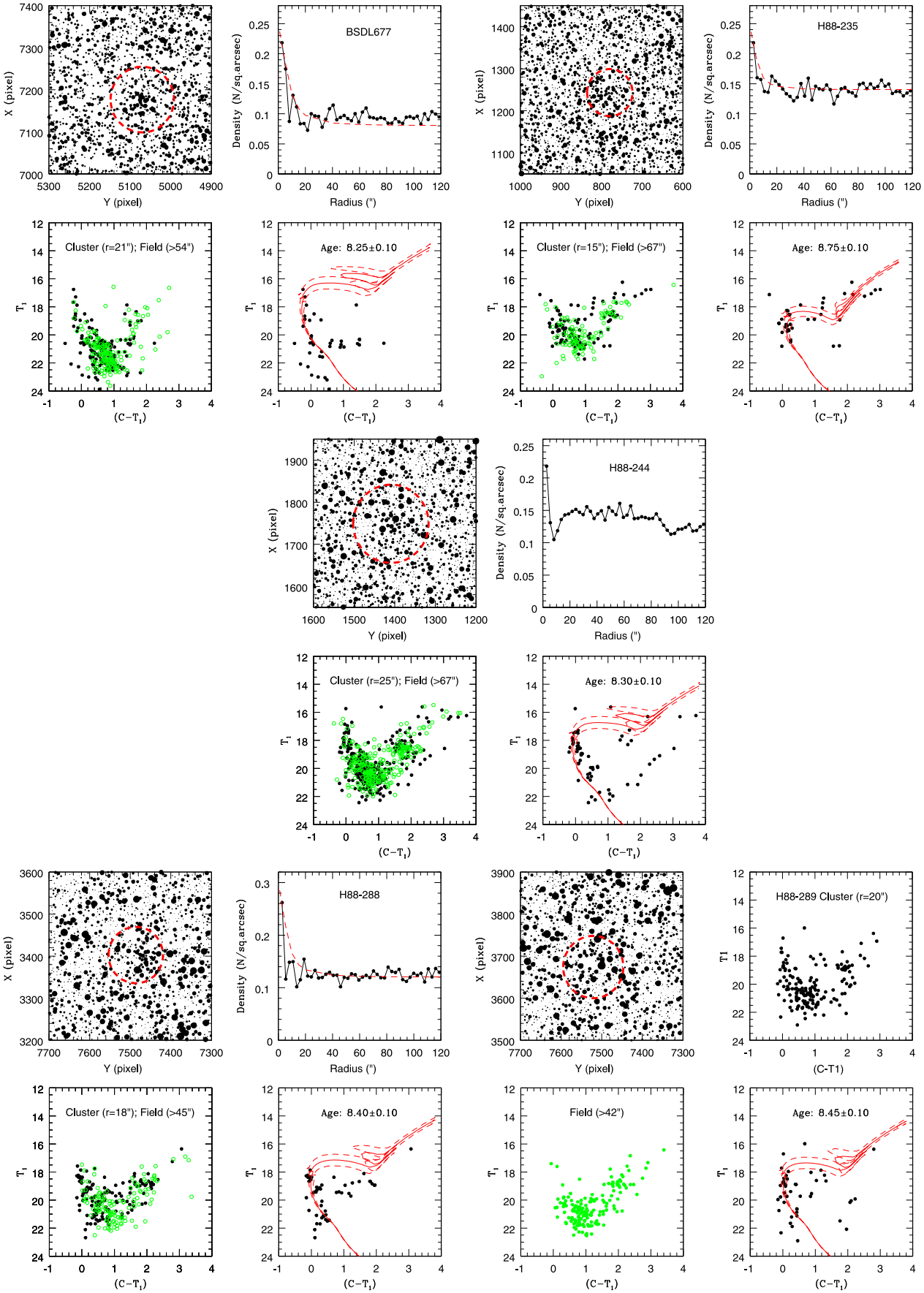

Figure C1. Possible clusters/asterisms: for BSDL677, H88-235, H88-244, and H88-288 the panel description is the same as for Figure 1, except that in the case of H88-244, no King profile fit to RDP is shown. For H88-289 the top right panel shows the CMD of stars within the estimated cluster radius (black filled circles), whereas the bottom left panel shows the CMD of the annular field (green filled circles). The top left and bottom right panel descriptions for H88-289 are the same as for Figure 1.

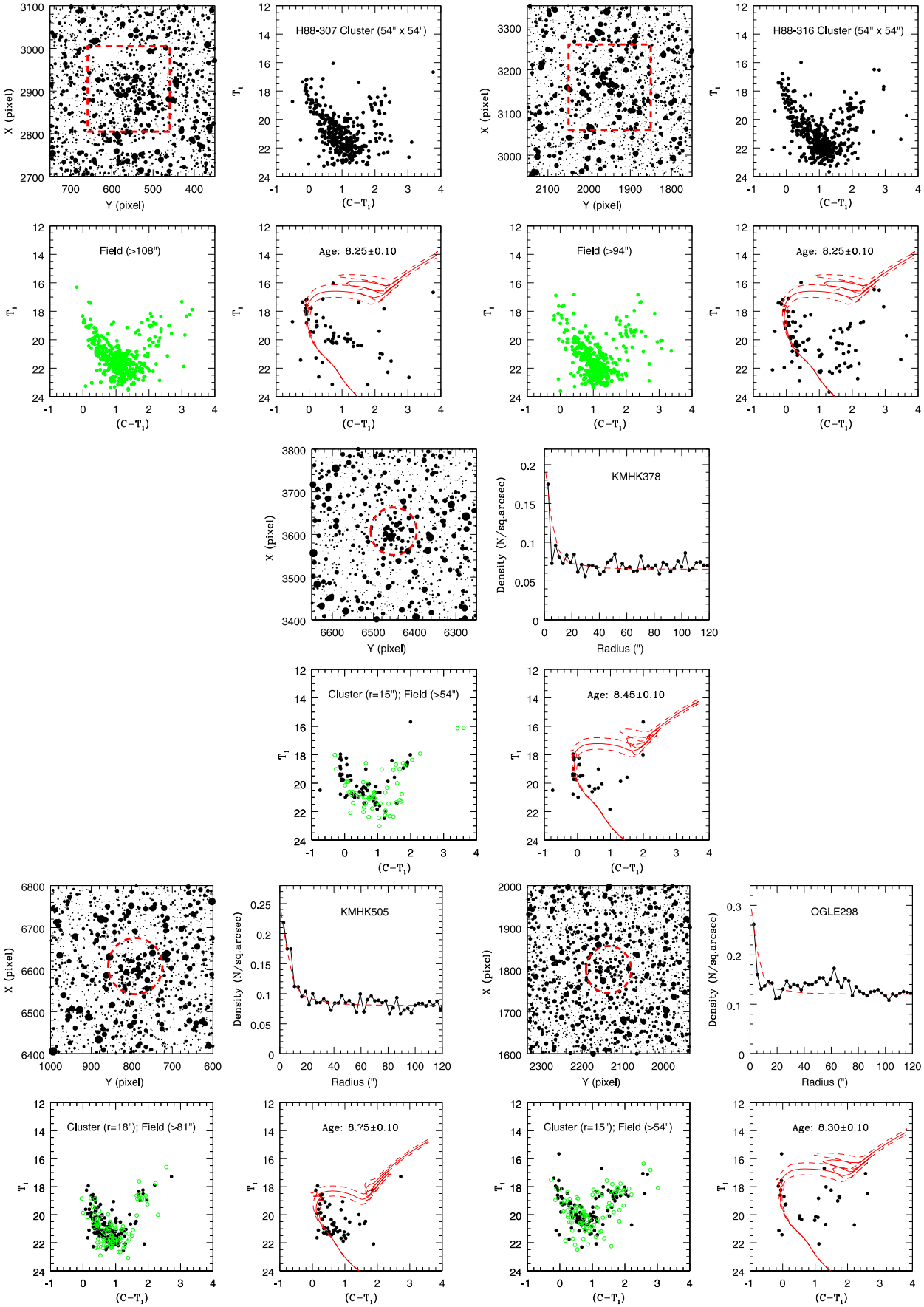

Figure C2. Possible clusters/asterisms: for KMHK 378, KMHK505, and OGLE 298 the panel description is the same as for Figure 1. For H88-307 and H88-316 the top right panel shows the CMD of stars within the estimated cluster size (black filled circles), whereas the bottom left panel shows the CMD of the annular field (green filled circles). The top left and bottom right panel descriptions are the same as for Figure 1.

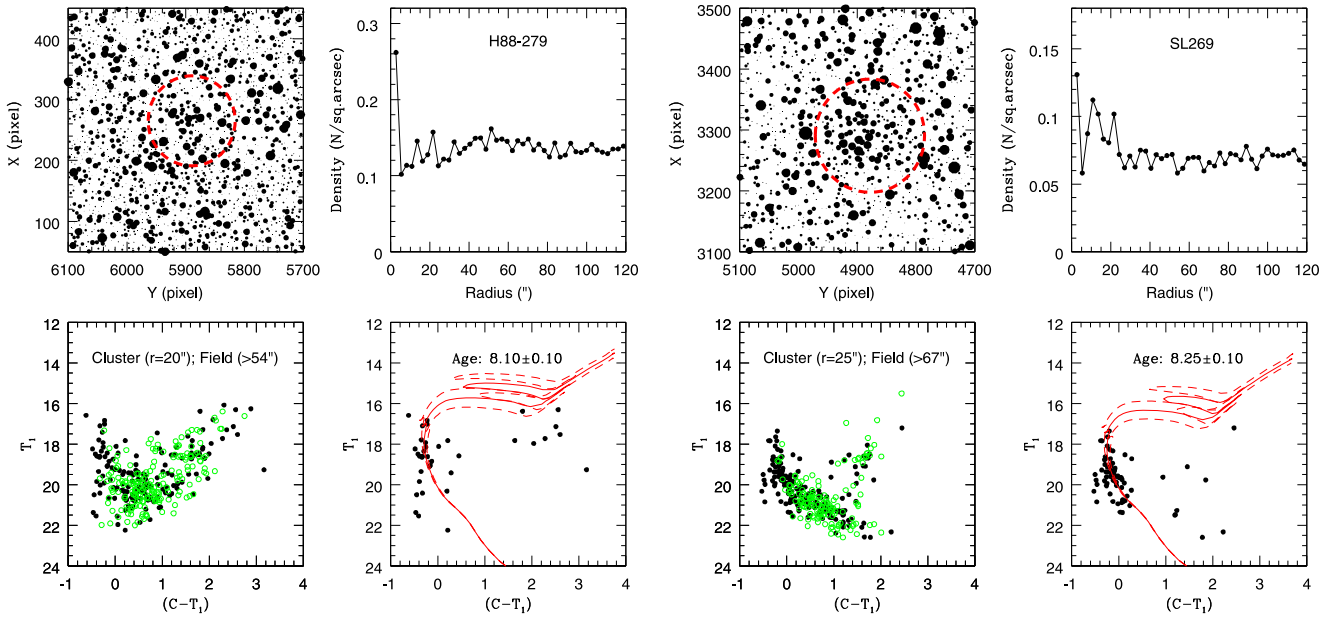

Figure C3. Possible clusters/asterisms: for H88-279 and SL 269, the panel description is the same as for Figure 1, except that for both cases, no King profile fit is shown.

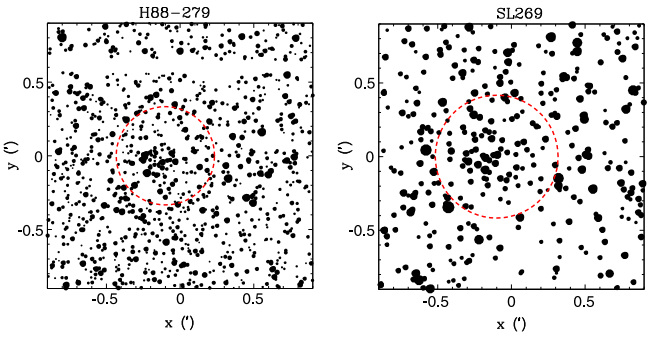

Figure C4. The OGLE III schematic charts for H88-279 and SL 269. The red dashed circles correspond to their derived size using our Washington data.

H88-306 ($5^h\ 40^m\ 24^s$, $-69^\circ\ 15'\ 10''$). B08 lists BSDL2768 as an association. G10 gives an estimation of its age as ∼60 Myr ($\log(t) = 7.80$, with $0.30 \leqslant$ error <0.50). For H88-306, Piatti (2014) estimated an age of ∼125 Myr ($\log(t) = 8.10 \pm 0.10$). The coordinates of both BSDL2768 and H88-306 suggest that they could lie within the estimated area for the central cluster H88-307. However, given the broad and marginally dense stellar distribution, coupled with similar SFH with respect to the field, we are not able to detect, identify, and estimate the parameters for each of these clusters individually.

6. H88-316: the spatial plot indicates an asymmetric distribution of bright stars around the expected cluster center. The cluster and the field regions show similar features in the CMD, thus posing difficulty to efficiently identify the presence of a cluster and estimate its corresponding parameters. The center of the cluster field (as mentioned in B08 catalog) is chosen as the cluster center. By comparing the CMDs of the central region with field regions at different annular radii, we conclude that there could be a cluster located within an area of ($54'' \times 54''$) around the cluster center. The poor MS feature (brighter than 19.0 mag and bluer than 0.4 mag) identified in the central region is found to be ∼180 Myr ($\log(t) = 8.25 \pm 0.20$), suggesting that if a cluster is present at all, it is a poor and young one, located within the mentioned area. The age for this cluster has been previously estimated by G10 as ∼100 Myr (i.e., $\log(t) = 8.00$, with $0.30 \leqslant$ error <0.50), whereas P12 estimated the cluster to be much younger, ∼18 Myr ($\log(t) = 7.27^{+0.30}_{-0.17}$). Our age estimation agrees well with that of G10, within the errors.
7. KMHK 378: the spatial distribution shows a small and feebly enhanced stellar distribution spot near the central region. The CMD extracted within the estimated cluster radius ($15''$) shows a poor upper MS (brighter than 20.0 mag and bluer than 0.4 mag), which could belong to the cluster. The MS feature does not get prominent for larger radii and is retained even after field star subtraction. The bright upper MS stars are found to be compactly distributed around the cluster center. Thus there is a possibility that KMHK 378 is a small, poor, and young (∼280 Myr i.e., $\log(t) = 8.45 \pm 0.20$) cluster candidate. According to Dieball et al. (2002), another cluster, KMHK 372, is present in the same field, with coordinates ($4^h\ 58^m\ 07^s$, $-69^\circ\ 48'\ 16''$), whereas B08 lists it as an association. The age estimated by G10 for KMHK 378 is ∼25 Myr ($\log(t) = 7.40$, error $\leqslant 0.30$) and is very similar to that estimated by P12, $\log(t) = 7.37^{+0.12}_{-0.14}$. For KMHK 372, G10 estimated an age of ∼250 Myr ($\log(t) = 8.40$, with $0.30 \leqslant$ error <0.50). Given its coordinate, KMHK 372 could lie within the estimated radius of KMHK 378. However, looking at the spatial plot, it is difficult to identify them individually, considering the density distribution near the center is very poor. It is probable that we are estimating the parameters for KMHK 378 and KMHK 372 put together.
8. KMHK 505: marginal density enhancement around the cluster center is observed in the spatial plot, which corresponds to a peak in the RDP within a radius of $18''$. The cluster feature extracted within this estimated radius

shows a poor and broad upper MS (brighter than 20.0 mag and bluer than 1.0 mag). The feature stays even after field star subtraction. A spatial distribution of these upper MS stars shows a density enhancement at the location of the cluster. The corresponding OGLE III field does not show any significant density enhancement within the cluster region. The reason could be the age of this cluster and the absence of bright giants. Based on our analysis we infer that KMHK 505 could be a poor, small, and young (~560 Myr) possible cluster candidate.

9. OGLE 298: the spatial plot of OGLE 298 appears very homogeneous, without any significant density enhancement near the expected cluster center. The center of the cluster field (as mentioned in B08 catalog) is chosen as the cluster center, and the CMD extracted within the estimated cluster radius (15″) seems to show a very poor upper MS (brighter than 19.0 mag and bluer than 0.4 mag), which may belong to the cluster. However, the spatial distribution of the bright upper MS stars does not show any significant density enhancement at the location of the cluster and looks almost homogeneous. Feeble cluster features, similarity between field and cluster CMDs, as well as large amount of differential reddening within the OGLE 298 cluster field, makes it inconvenient to efficiently identify the presence of the cluster. The estimated reddening for this cluster is about 0.25 mag, much higher than the reddening of the corresponding field, which is 0.10 mag. We conclude that if a cluster exists at all, it is a very small, poor, and young (~200 Myr i.e., $\log(t) = 8.30 \pm 0.20$) one. The cluster has been previously studied by PU00, who claim the cluster to be much younger (~20 Myr i.e., $\log(t) = 7.30 \pm 0.20$). We detect only one bright MS star and could possibly derive a younger age if we consider it as a cluster member.
10. H88-279: the spatial plot of H88-279 appears quite homogeneous, with no significant density enhancement near the expected center of the cluster. We considered an area of (54″ × 54″) around the central region of the observed field. Comparison of the CMD of the suspected cluster region and different field regions helped in identifying a poor cluster MS, brighter than 19.0 mag and bluer than 0.2 mag. For cluster areas greater than the above value, there is no change in the observed cluster MS. This suggests that there may be a cluster in the suggested location. In order to locate the cluster center, we made a spatial distribution of the bright upper MS stars and found a small compact distribution of them near the suspected cluster location. The cluster MS in the CMD was found to be well-populated, including stars within 20″ radius. At larger radii there is not much change observed in the extracted cluster feature. In order to cross-check the presence of a young cluster in this field we extracted OGLE III data corresponding to this cluster, having similar area as our data. This schematic chart shows a feeble density enhancement due to bright stars around the cluster center (Figure C4). We thus suggest that H88-279 is possibly a small, poor, and young (~125 Myr, i.e., $\log(t) = 8.10 \pm 0.20$) cluster candidate. Earlier study by PU00 using OGLE II data mentioned an age of ~100 Myr ($\log(t) = 8.00 \pm 0.10$), whereas P12 estimated a relatively younger age of ~74 Myr ($\log(t) = 7.87^{+0.06}_{-0.04}$). Our estimation is in good agreement with G10 and in moderate agreement with P12, within the errors.
11. SL 269: the central region of the cluster does not look compact but instead dispersed, resulting in an uneven RDP. An upper MS (brighter than 20.0 mag and bluer than 0.2 mag) is observed when the CMDs of the cluster and the field region are compared. The cluster radius is selected to be the one (25″) at which the upper MS becomes well-populated. It is observed that the cluster feature stays and appears prominent even after field star subtraction. A spatial distribution of these upper MS stars shows a density enhancement at the location of the cluster. The cluster is a young one, and the corresponding OGLE III field (Figure C4) shows a marginal density enhancement within the cluster region. We conclude that SL 269 may be a poor, small, and young (~180 Myr) possible cluster candidate.

REFERENCES

Baumgardt, H., Parmentier, G., Anders, P., & Grebel, E. K. 2013, MNRAS, 430, 676
Bessell, M. S., & Brett, J. M. 1988, PASP, 100, 1134
Bica, E., Bonatto, C., Dutra, C. M., & Santos, J. F. C., Jr. 2008, MNRAS, 389, 678
Bonatto, C., Ortolani, S., Barbuy, B., & Bica, E. 2010, MNRAS, 402, 1685
Canterna, R. 1976, AJ, 81, 228
Dieball, A., Müller, H., & Grebel, E. K. 2002, A&A, 391, 547
Geisler, D. 1996, AJ, 111, 480
Geisler, D., Bica, E., Dottori, H., et al. 1997, AJ, 114, 1920
Geisler, D., & Sarajedini, A. 1999, AJ, 117, 308
Glatt, K., Grebel, E. K., & Koch, A. 2010, A&A, 517, A50
Grocholski, A. J., Cole, A. A., Sarajedini, A., Geisler, D., & Smith, V. V. 2006, AJ, 132, 1630
Hunter, A. D., Elmegreen, B. G., Dupuy, T. J., & Mortonson, M. 2003, AJ, 126, 1836
Jannuzi B.T., Claver J., & Valdes F. 2003, The NOAO Deep Wide-Field Survey MOSAIC Data Reductions, http://www.noao.edu/noao/noaodeep/ReductionOpt/frames.html
King, I. 1962, AJ, 67, 471
Marigo, P., Girardi, L., Bressan, A., et al. 2008, A&A, 482, 883
Olszewski, E. W., Schommer, R. A., Suntzeff, N. B., & Harris, H. C. 1991, AJ, 101, 515
Palma, T., Clariá, J. J., Geisler, D., Piatti, A. E., & Ahumada, A. V. 2013, A&A, 555, A131
Piatti, A. E. 2011, MNRAS, 418, L40
Piatti, A. E. 2012, A&A, 540, A58
Piatti, A. E. 2014, MNRAS, 440, 3091
Piatti, A. E., Bica, E., Geisler, D., & Clariá, J. J. 2003, MNRAS, 344, 965
Piatti, A. E., Clariá, J. J., Parisi, M. C., & Ahumada, A. V. 2011, PASP, 123, 519
Piatti, A. E., & Geisler, D. 2013, AJ, 145, 17
Piatti, A. E., Geisler, D., Sarajedini, A., & Gallart, C. 2009, A&A, 501, 585
Pietrzyński, G., & Udalski, A. 2000, AcA, 50, 337
Popescu, B., Hanson, M. M., & Elmegreen, B. G. 2012, ApJ, 751, 122
Saha, A., Olszewski, E. W., Brondel, B., et al. 2010, AJ, 140, 1719
Stetson, P. B., Davis, L. E., & Crabtree, D. R. 1990, in ASP Conf. Ser. 8, CCDs in Astronomy, ed. G. H. Jacoby (San Francisco: ASP), 289
Subramaniam, A., & Subramanian, S. 2010, A&A, 520, A24
Udalski, A., Soszyński, I., Szymański, M. K., et al. 2008, AcA, 58, 89
Zaritsky, D., Harris, J., Thompson, I. B., & Grebel, E. K. 2004, AJ, 128, 1606